JOURNAL OF GEOPHYSICAL RESEARCH, VOL. 112, D10S17, doi:10.1029/2006JD007602, 2007

Contribution of gas phase oxidation of volatile organic compounds to atmospheric carbon monoxide levels in two areas of the United States

Robert J. Griffin,[1,2] Jianjun Chen,[1] Kevin Carmody,[3] Satish Vutukuru,[3] and Donald Dabdub[3]

Received 31 May 2006; revised 18 December 2006; accepted 30 January 2007; published 18 April 2007.

[1] Three-dimensional modeling studies have been performed to investigate the short-timescale photochemical generation of carbon monoxide (CO) on a regional basis in two very distinct areas of the United States: New England (mixed biogenic and anthropogenic influence) and the South Coast Air Basin (SoCAB, dominated by anthropogenic influence) of California. For the New England study, the Caltech Atmospheric Chemistry Mechanism (CACM) was incorporated into the Community Multiscale Air Quality model and applied to 3–4 August 2004. For the SoCAB, CACM was applied to 8–9 September 1993 using the California Institute of Technology three-dimensional regional atmospheric model. Results indicate that in each location, on a relative scale, the photochemical generation of CO is responsible for less than 10% (3–9% for the eastern United States and approximately 1% in the SoCAB) of the total simulated mixing ratio for the respective dates based on domain-wide, calendar-based 24-hour averages. In the eastern United States, simulations indicate that isoprene is the major volatile organic compound (VOC) source for CO and that VOC oxidation can lead to up to approximately 20 parts per billion by volume (ppb) of CO in New England. In the SoCAB, anthropogenic short-chain alkenes lead to the greatest amount of photochemical CO generation; VOC oxidation in its entirety can lead to up to approximately 45 ppb of photochemically generated CO in the SoCAB. Therefore studies on the regional scale that use CO as a marker of primary combustion emissions may overestimate the importance of primary emissions, depending on location and time.

Citation: Griffin, R. J., J. Chen, K. Carmody, S. Vutukuru, and D. Dabdub (2007), Contribution of gas phase oxidation of volatile organic compounds to atmospheric carbon monoxide levels in two areas of the United States, *J. Geophys. Res.*, *112*, D10S17, doi:10.1029/2006JD007602.

1. Introduction

[2] Carbon monoxide (CO) is one of the most important trace gases in the troposphere. It is a species that affects the mixing ratios of atmospheric hydroxyl radicals (OH) because of their reaction in the presence of molecular oxygen (O_2):

$$\text{(R1)} \qquad CO + OH + O_2 \rightarrow CO_2 + HO_2$$

On the basis of this reaction, the atmospheric lifetime of CO is approximately two months [*Seinfeld and Pandis*, 2006]. OH is the dominant tropospheric oxidant responsible for consumption of volatile organic compounds (VOCs); therefore CO and VOC levels are linked intricately. This link also exists because the atmospheric oxidation of VOCs leads to the formation of CO, as discussed subsequently.

[3] Reaction (R1) shows that CO oxidation by OH produces not only carbon dioxide (CO_2), a known greenhouse gas, but also the hydroperoxide radical (HO_2). HO_2 converts nitric oxide to nitrogen dioxide in the cycle that leads to production of photochemical ozone (O_3):

$$\text{(R2)} \qquad HO_2 + NO \rightarrow OH + NO_2$$

In addition, the United States Environmental Protection Agency (USEPA) lists CO as a criteria pollutant for which National Ambient Air Quality Standards have been established (eight-hour standard of 9 parts per million (ppm) and one-hour standard of 35 ppm) because of its known health effects upon inhalation.

[4] In addition, measurements of CO have been used to approximate photochemical air mass age [*Fishman and Seiler*, 1983], to infer pollution sources [*de Reus et al.*, 2003], to estimate the export of photochemical pollution on the continental to hemispheric scale [*Anderson et al.*, 1993; *Chin et al.*, 1994; *Parrish et al.*, 1998; *Mao and Talbot*, 2004], and to calculate the O_3 production efficiency (OPE)

[1] Climate Change Research Center, University of New Hampshire, Durham, New Hampshire, USA.
[2] Also at Department of Earth Sciences, University of New Hampshire, Durham, New Hampshire, USA.
[3] Department of Mechanical and Aerospace Engineering, University of California, Irvine, California, USA.

0148-0227/07/2006JD007602$09.00

at a given time and location [*Fishman and Seiler*, 1983; *Griffin et al.*, 2004]. Therefore it is critical to understand the sources that contribute to the tropospheric burden of this important trace gas.

[5] CO has both natural and anthropogenic sources, as reviewed by *Seinfeld and Pandis* [2006] and *Kanakidou and Crutzen* [1999]. Primary natural sources of CO include soil, plants, and the ocean; primary anthropogenic sources of CO include combustion of fossil fuel. Biomass burning, which could be considered either anthropogenic or natural depending on cause of the fire, also contributes significantly to emissions of CO to the atmosphere. In addition to primary sources, CO is formed photochemically in the atmosphere or in snow, after which it is released to the atmosphere [*Haan et al.*, 2001]. As summarized by *Kanakidou and Crutzen* [1999], for example, methane (CH_4) oxidation is known to contribute to CO on the global scale after it is oxidized by OH. Oxidation of non-CH_4 VOCs (anthropogenic and biogenic, including those that contain functional groups, particularly alcohols and aldehydes) also contributes to the levels of CO in the atmosphere. This oxidation sequence can be initiated, depending on VOC molecular structure, by OH, O_3, the nitrate radical (NO_3), or the oxygen atom (O).

[6] On the global scale, the contributions of the oxidation of CH_4 and VOCs (both anthropogenic and biogenic) to CO levels have been quantified using a variety of models [*Zimmerman et al.*, 1978; *Khalil and Rasmussen*, 1990; *Taylor et al.*, 1996; *Houweling et al.*, 1998; *Kanakidou and Crutzen*, 1999; *Granier et al.*, 2000; *Poisson et al.*, 2000]. These studies indicate that 22–40% of the total annual global CO source (including direct emissions and photochemical production) is related to oxidation of CH_4. Most estimates are on the lower end of this range. *Khalil and Rasmussen* [1990] indicated an approximately equal contribution to photochemical CO generation from natural and anthropogenic sources of CH_4.

[7] Similarly, most of these global modeling studies estimate that approximately 20% of the global annual CO source results from oxidation of non-CH_4 VOCs, with a range of 14 to 44%. Biogenic influences are generally four to five times greater than those of anthropogenic species for the non-CH_4 VOC contribution to CO formation. Contributions to CO levels are most important during summer and relatively close (on the global scale) to the VOC emission sources. Similar global-scale studies have been performed and indicate a high conversion of reactive carbon compounds to CO_2 that is formed partially via the CO pathway described by the CO reaction with OH (reaction (R1)) [*Folberth et al.*, 2005].

[8] Far fewer studies have investigated the effect of VOC oxidation on atmospheric CO levels on the local to regional scale. Simulations pertaining to the Aerosol formation from Biogenic organic Carbon (AEROBIC) campaign in a forested region of central Greece in the summer of 1997 indicate that oxidation of biogenic VOCs (isoprene and monoterpenes) can lead to photochemical formation of CO at a rate in the range of 1 to 3 parts per billion (ppb) per hour [*Gros et al.*, 2002; *Tsigaridis and Kanakidou*, 2002]. This rate of photochemical CO formation often exceeded the local anthropogenic mass emission rate converted to a growth rate in the mixing ratio. Field studies, for example over the Amazon, also indicate that oxidation of biogenic VOCs is likely a cause of increased CO with decreased elevation during the wet season [*Harriss et al.*, 1990].

[9] This study conducts for the first time detailed simulations to assess the contribution of VOC oxidation to CO on the regional and urban scales. The contribution of VOC oxidation to CO levels in the eastern United States, including areas influenced strongly by emissions of biogenic hydrocarbons as well as major metropolitan areas such as New York City, New York; Boston, Massachusetts; and Washington, D. C., is investigated here. Specific focus is placed on New England because of the importance of this region for pollutant transport across the Atlantic Ocean [*Anderson et al.*, 1993; *Chin et al.*, 1994; *Parrish et al.*, 1998; *Mao and Talbot*, 2004]. New England also is influenced by pollution sources in the Midwestern United States. The time period for this investigation (3–4 August 2004) coincides with a portion of the International Consortium for Atmospheric Research on Transport and Transformation (ICARTT) (1 July to 15 August 2004) field campaign [*Fehsenfeld et al.*, 2006]. ICARTT was a multinational, multiagency large measurement, modeling, and forecast campaign aimed at characterizing the atmospheric processes that control the spatial and temporal profiles of air pollutants such as O_3 and aerosols in New England. CO data collected in New England during the ICARTT campaign are used during this study.

[10] A similar study is performed for the South Coast Air Basin (SoCAB) of California, where anthropogenic emissions are dominant. The SoCAB is an area that experiences among the worst air quality in the United States. Simulations are presented for a 2-day photochemical pollution episode that occurred 8–9 September 1993. The dates are selected on the basis of a rich supporting available data set. Namely, during this 2-day period, an intensive field monitoring program was conducted with the main goal of identification and quantification of organic species in the gas and particles phases; ancillary data, including CO mixing ratios, were collected for use in air quality model evaluation [*Fraser et al.*, 1996].

2. Methods

2.1. Model Applications

2.1.1. Model Description

[11] The gas phase chemical mechanism used in the present study is the Caltech Atmospheric Chemistry Mechanism (CACM) [*Griffin et al.*, 2002a]. CACM uses a lumped (based on structures, reaction rate constants with OH, and secondary organic aerosol (SOA) yield) surrogate approach for VOCs and tracks individual products of the chosen surrogate compounds. The model solves kinetic rate expressions for over 120 different species. While the development of CACM was motivated by the desire to simulate SOA formation, particular attention was also paid to the chemistry of VOCs containing fewer than six carbon atoms, CO, and oxides of nitrogen so that O_3 prediction is possible. The version of CACM used in the current study incorporates all changes outlined by *Griffin et al.* [2005] but does not include the updated monoterpene chemistry simulated by *Chen and Griffin* [2005] because monoterpenes are expected to have a significantly smaller influence in the SoCAB. CACM is an intermediate

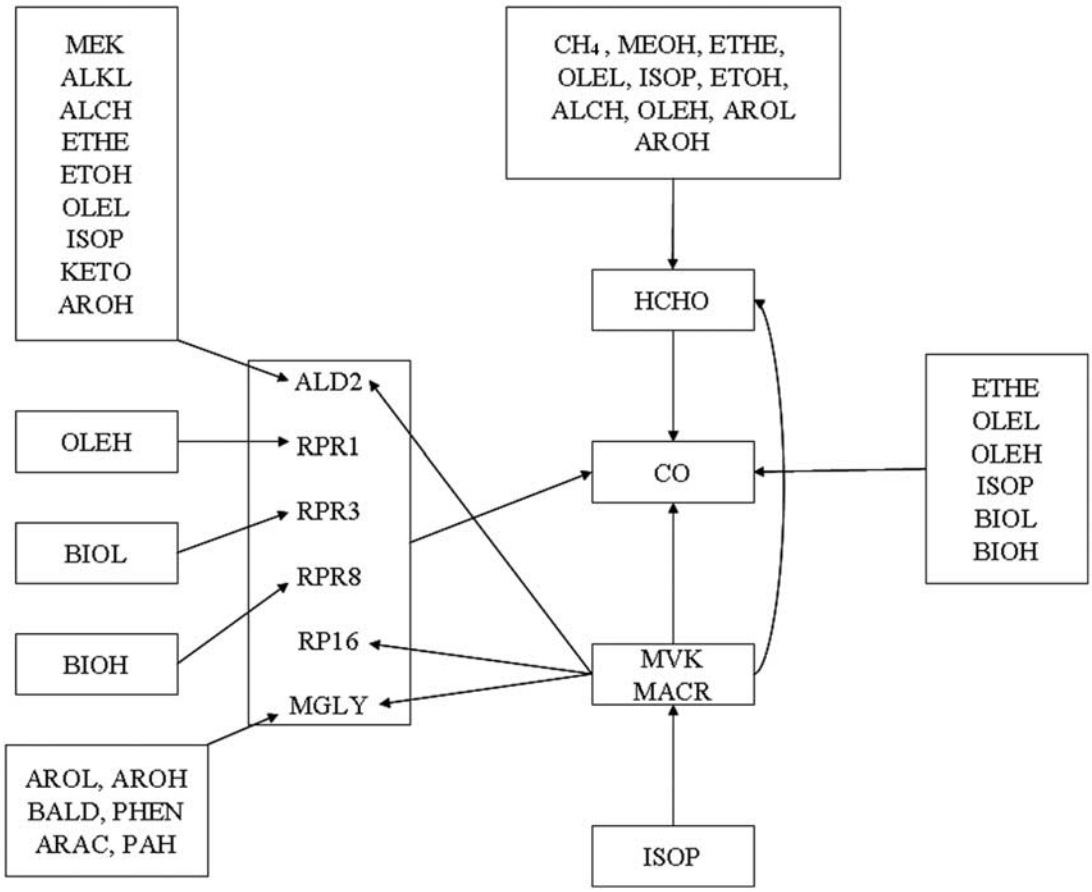

Figure 1. Secondary routes of CO formation within CACM. Chemical species names refer to *Griffin et al.* [2002a] and are described in the text and Table 1.

approach between less specific chemical mechanisms such as Carbon Bond IV (CB-IV) [*Gery et al.*, 1989] and the completely specified Master Chemical Mechanism [see, e.g., *Jenkin et al.*, 2003]. Such an intermediate approach allows a balance between chemical detail and computational demand.

2.1.2. Chemical Generation of CO in CACM

[12] Within CACM, several chemical pathways lead to the formation of CO via secondary photochemical routes, as shown in Figure 1. Species names used in Figure 1 and in the text are summarized in Table 1. Primary species for which CO is considered a first-generation product include HCHO, ALD2, ETHE, OLEL, OLEH, ISOP, BIOL, and BIOH. Each of these species besides HCHO and ALD2 is characterized by unsaturated carbon-carbon bonds and leads directly to CO via reaction with O and O_3. HCHO and ALD2 lead to CO formation via photolysis; HCHO also forms CO via reaction with NO_3 and OH.

Table 1. Species List and Names Associated With CACM and Relevant to Photochemical CO Generation

Species	Description	Species	Description
CH_4	methane	AROL	low-SOA-yield aromatics
HCHO	formaldehyde	AROH	high-SOA-yield aromatics
MEOH	methanol	PAH	polycyclic aromatic hydrocarbons
ETHE	ethene	BALD	aldehydic aromatics
ETOH	ethanol	PHEN	phenolic compounds
ALKL	small-carbon-number alkanes	ARAC	aromatic acids
OLEL	small-carbon-number alkenes	MVK	methyl-vinyl ketone (oxidation product of ISOP)
MEK	small-carbon-number ketones	MACR	methacrolein (oxidation product of ISOP)
KETO	large-carbon-number ketones	RPR1	aldehydic oxidation product of OLEH
ALD2	higher aldehydes	RPR3	aldehydic oxidation product of BIOL
ALCH	higher alcohols	RPR8	aldehydic oxidation product of BIOH
OLEH	large-carbon-number alkenes	RP16	aldehydic oxidation product of MVK and MACR
ISOP	isoprene	MGLY	aldehydic oxidation product of MVK, MACR, and several aromatic species
BIOL	low-SOA-yield monoterpenes		
BIOH	high-SOA-yield monoterpenes		

[13] Several secondary aldehydic species in CACM also lead to the formation of CO upon photolysis. These include RPR1, RPR3, RPR8, RP16, and MGLY. MGLY is a second-generation oxidation product of ISOP because it is formed during the oxidation of first-generation products MVK and MACR. MGLY is also a ring-fragmentation product of several aromatic species. ALD2 is also a secondary species in CACM and is formed by oxidation of MVK, MACR, ETHE, OLEL, ISOP, AROH, MEK, KETO, ALKL, ETOH, and ALCH. CO is also a direct product of the oxidation of MVK and MACR.

[14] Several species also lead to HCHO, which in turn is converted to CO, as discussed above. These include the secondary species MVK and MACR and the primary species MEOH, ETOH, ETHE, OLEL, ALCH, OLEH, ISOP, AROL, AROH, and CH_4. However, in base case modeling for both the eastern United States and the SoCAB, the mixing ratio of CH_4 is set to a constant, with this value being 1.85 ppm for the eastern United States and 2.2 ppm for the SoCAB, respectively.

2.1.3. Three-Dimensional Applications

[15] For simulation of the air quality in the eastern United States, CACM is implemented into the Community Multi-scale Air Quality (CMAQ) model version 4.4 [*Byun and Ching*, 1999; *Binkowski and Roselle*, 2003] and applied to a domain that extends from the Gulf of Mexico in the southwest, to Minnesota in the northwest, and to the Canadian maritime provinces in the northeast (Figure 2a). CMAQ with CACM incorporated is applied to 3 and 4 August 2004 (UTC) with 2 days of spin-up. These dates were part of the ICARTT campaign. Application of CACM for simulation of SOA during this time period is described in detail by *Chen et al.* [2006], as are details regarding model performance for O_3, particulate matter mass, and individual particulate matter species concentrations. Emission profiles have been processed with the Sparse Matrix Operator Kernel Emissions (SMOKE1.0) system as in the work by *Mao et al.* [2006]. Meteorological fields were simulated with the PSU/NCAR Mesoscale Modeling System Generation 5 version 3.4 (MM5), also as described by *Mao et al.* [2006]. The domain includes a 62 $\times$ 66 36-km horizontal grid and 21 vertical layers that are specified by a σ-pressure coordinate up to 10,000 Pa. The σ-pressure (σ) definition is:

$$\sigma = \frac{\left(P - P_{top}\right)}{\left(P_{surface} - P_{top}\right)} \tag{1}$$

where P is the actual pressure at the location, P_{top} is the pressure at the top of the domain (10,000 Pa), and $P_{surface}$ is the surface pressure defined by MM5. In this manner, σ has values that range from 1.0 at the surface to 0.0 at the top of the modeling domain. Model layers are defined according to the following series of σ points: 1.0, 0.9976, 0.9936, 0.9872, 0.979, 0.969, 0.957, 0.943, 0.927, 0.909, 0.889, 0.867, 0.843, 0.789, 0.727, 0.655, 0.56, 0.46, 0.36, 0.26, 0.14, and 0.0. Simulation results are shown at the surface for the entire domain and for the specific locations in New England of Thompson Farm (TF) in Durham, New Hampshire (semirural); Appledore Island (AI), Maine (marine area influenced by continental outflow); and Boston (BS), Massachusetts (urban). Additional base case data from other locations within the domain are also shown, but sensitivity case data are shown only for the entire domain and the specific locations in New England.

[16] For simulation of the SoCAB, the California Institute of Technology (CIT) three-dimensional regional air quality model is used [*Harley et al.*, 1993; *Meng et al.*, 1998]. Simulations are performed for 8 and 9 September 1993 with one initialization day, in a 30 $\times$ 80 5-km horizontal grid with five vertical layers extending to 1100 m. Moving in the vertical direction, the layers have depths of 13.0, 52.7, 153.9, 330.1, and 550.3 meters, respectively. The domain includes a portion of the Pacific Ocean in the west, the major urban areas associated with the city of Los Angeles, CA, and mountainous regions surrounding these urban areas (Figure 2b). Details on the CIT model, as well as relevant input parameters for this specific episode, are discussed by *Griffin et al.* [2002b]. Model results with respect to gas phase photochemical pollutants are also discussed by *Griffin et al.* [2002b]. In general, the model predicts primary pollutants at upwind locations and secondary pollutants at downwind locations adequately compared to observations. Secondary pollutants tend to be underpredicted at upwind locations. Simulation output is shown for central Los Angeles (CELA), an upwind site expected to be exposed heavily to primary emissions, Azusa (AZUS), a site further downwind subject to both primary emissions and secondary chemistry, and Riverside (RIVR), the site furthest downwind and expected to be influenced heavily by secondary chemistry. RIVR is approximately 100 km downwind of CELA. Assuming a typical boundary layer wind speed of 3 m s^{-1}, the transport time between the two locations is approximately nine hours.

[17] The effect of the chemistry of individual VOCs on CO is evaluated here by forcing emissions, boundary conditions (BCs), and initial conditions (ICs) for the species of interest to zero for each run, rather than using a labeling technique to track CO from individual pathways [*Kanakidou and Crutzen*, 1999; *Granier et al.*, 2000]. In this way, other feedbacks of the presence of the VOC (such as effects on OH and O_3 levels) are considered as part of the overall contribution to CO formation; the labeling technique does not allow for inclusion of this type of feedback. Most of the primary species discussed in conjunction with Figure 1 are considered for sensitivity runs for their secondary contribution to CO levels in each of the modeling domains. In addition, runs in which CO emissions, BCs, and ICs are set to zero are performed. This results in a total of 19 two-day simulations (base case plus 18 sensitivity runs) in each of the modeling domains for this comprehensive study. Sensitivity runs for MEOH, BALD, PHEN, and ARAC are not performed because of the very small emission rates for these compounds. In each of these simulations, model output generally is saved hourly while calculations are performed subhourly to satisfy stability criteria in the differential equation solvers used for transport and chemistry calculations. It should also be noted that the 2-day nature of the simulation is very short compared to the timescales associated with some of the relevant chemistry. Therefore the results presented should be interpreted only as being relevant

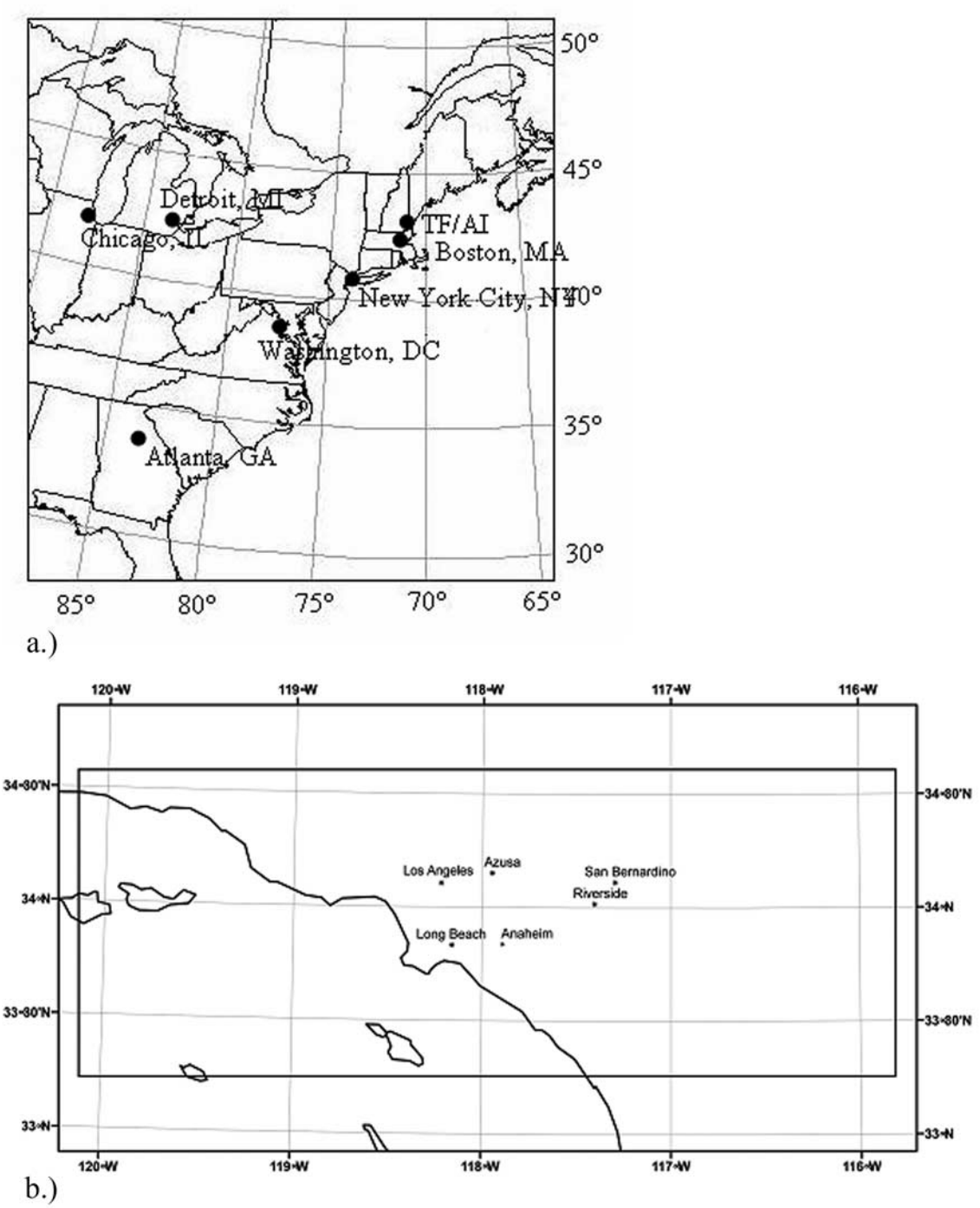

Figure 2. Domain maps for model simulations for (a) the eastern United States and (b) the South Coast Air Basin of California (inner box).

for the modeling domains and simulation dates presented here. Clearly there is the potential for additional secondary CO formation following air mass transport out of the domains used.

2.2. CO Measurements

[18] Data for CO at three locations in New England are used to show model capabilities and observed levels of CO. Data from TF and AI were generated by the AIRMAP program. AIRMAP CO measurement techniques focus on use of infrared spectroscopy and are detailed by *Mao and Talbot* [2004]. Here, 1-min average CO records for each site are averaged to one hour. Similar measurements were made in Boston, Massachusetts, by the USEPA, in the SoCAB by the South Coast Air Quality Management District, in the southeastern United States by the South-

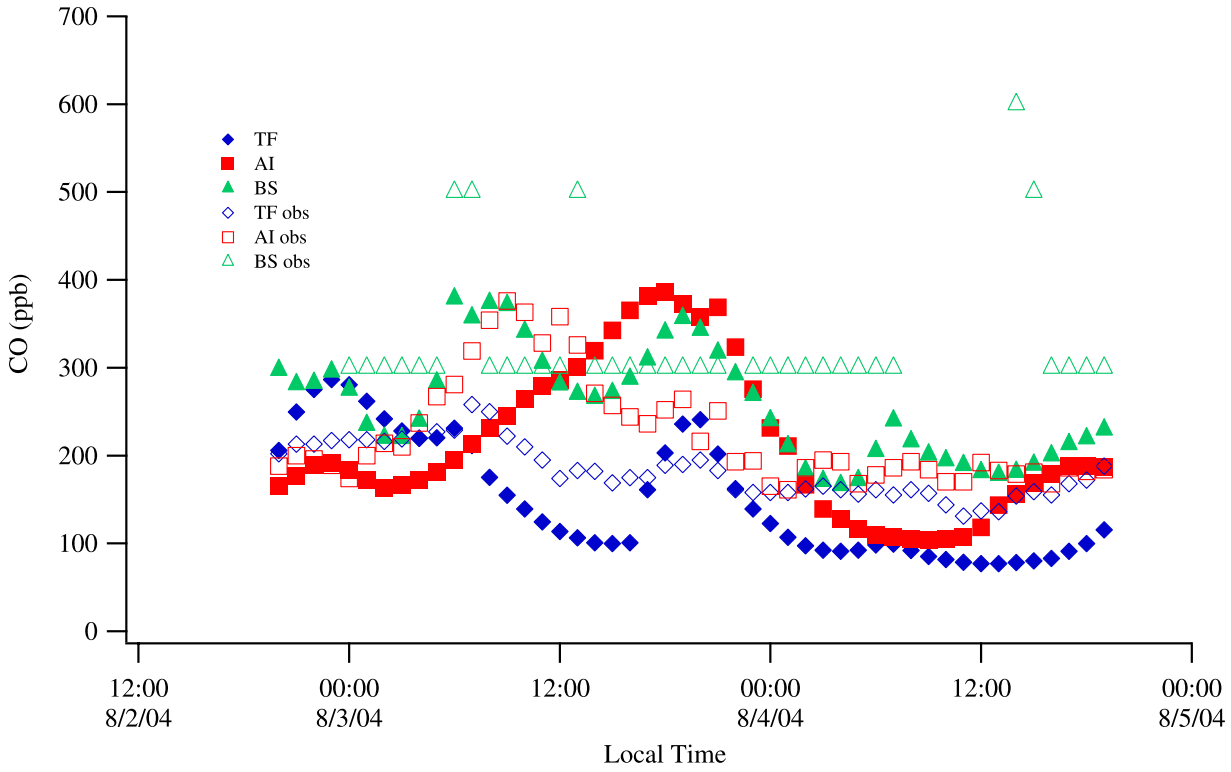

Figure 3a. Base case simulations and observations (obs) of CO mixing ratios in three locations in New England (TF, Thompson Farm; AI, Appledore Island; BS, Boston, Massachusetts).

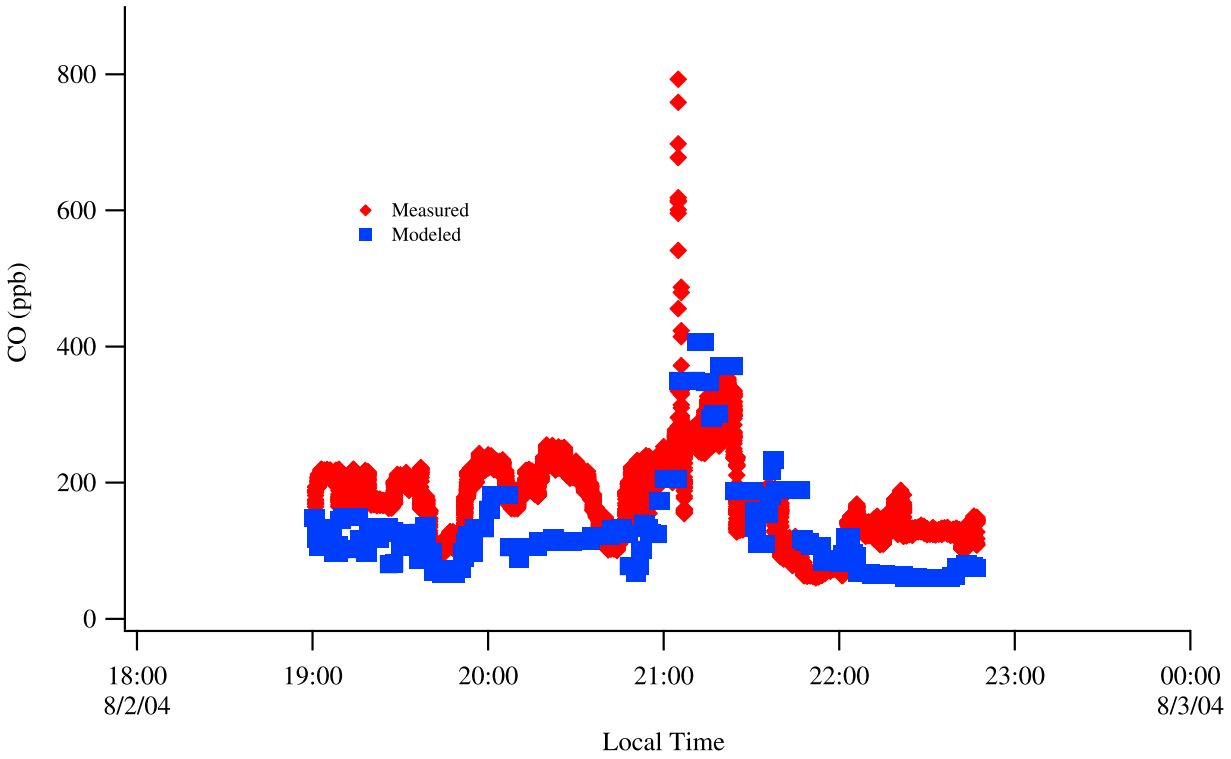

Figure 3b. Base case simulations and observations of CO mixing ratios from the NOAA P-3 aircraft.

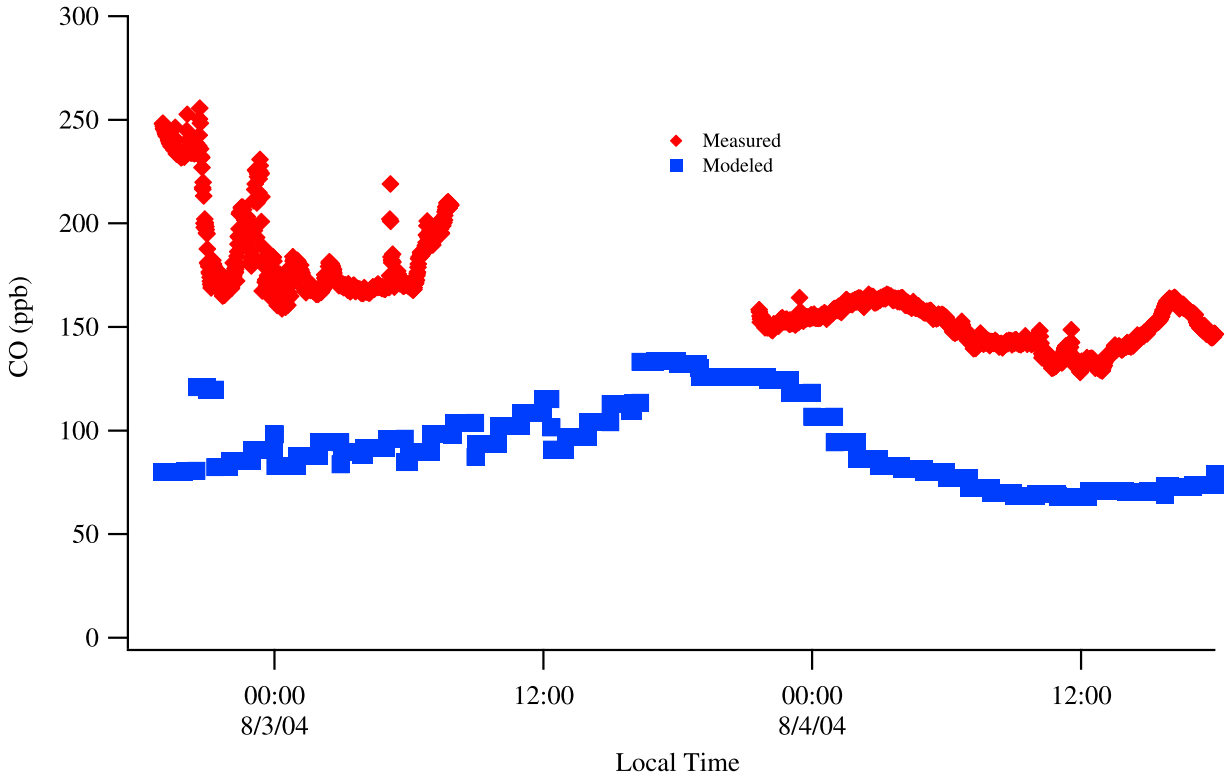

Figure 3c. Base case simulations and observations of CO mixing ratios from the NOAA Research Vessel *Ronald H. Brown*.

eastern Aerosol Research and Characterization (SEARCH) program [*Hansen et al.*, 2003], and on mobile National Oceanic and Atmospheric Administration (NOAA) platforms (airborne and ship-based) during ICARTT.

3. Results

3.1. Base Case Results

[19] Simulated CO mixing ratios from the base case for the locations of interest within each domain are shown in Figure 3. For this discussion, all simulation results are presented for model surface grid boxes only, except for comparison to data from the NOAA P-3 aircraft. Output is also compared to available AIRMAP observations from TF and AI, to USEPA measurements in Boston, Massachusetts, to SEARCH measurements in rural Georgia and urban Atlanta, Georgia, and to measurements made on the NOAA Research Vessel *Ronald H. Brown*.

[20] At TF, the model shows a general underprediction for 3 and 4 August 2004, as shown in Figure 3a. The absolute peak mixing ratio values at AI are well predicted by the model. However, there is a more significant issue with regard to timing of this peak. Because the amplitude of this peak is matched adequately, it is presumed that the issues with timing result from inaccuracies in the simulated transport pathways between BS and AI because AI appears to be influenced by plumes from BS regularly (M. White et al., Volatile organic compound measurements at Thompson Farm, New Hampshire, and Appledore Island, Maine: A comparison of relative reactivities and variability, unpublished manuscript, 2007, hereinafter referred to as White et al., unpublished manuscript, 2007). Simulations for BS are characterized by peaks at approximately 0800 and 2000 local time. The peaks predicted in the morning are larger than those predicted for the evening. It is difficult to make comparisons between observations and simulations for BS because the data for the downtown BS site have been rounded to the nearest tenth of a ppm. Such a comparison, however, indicates that the correct order of magnitude is achieved for simulation of CO in BS on these dates. For the fixed New England locations, simulated peak mixing ratios are highest at BS and AI (up to approximately 400 ppb) and lower at TF (up to approximately 300 ppb), indicative of the fact that the offshore location of AI makes it more susceptible to influence from the BS urban plume [*Mao and Talbot*, 2004; White et al., unpublished manuscript, 2007].

[21] Additional measurements of CO were performed during ICARTT on mobile platforms, including the NOAA P-3 aircraft and the Research Vessel *Ronald H. Brown.* The aircraft flight plan on 3 August 2004 focused on southern New England; New York City, New York; New Jersey; and Long Island, with an altitude up to approximately 3 km. Only limited data are available for this date from the P-3 because of a shortened flight period. For comparison to this data, plane location was used to determine the horizontal grid cell. The reported pressure altitude was converted to σ-pressure to determine the appropriate model layer. A comparison between observations and modeled output for the P-3 is given in Figure 3b. The simulation of the data from the P-3 is acceptable, in

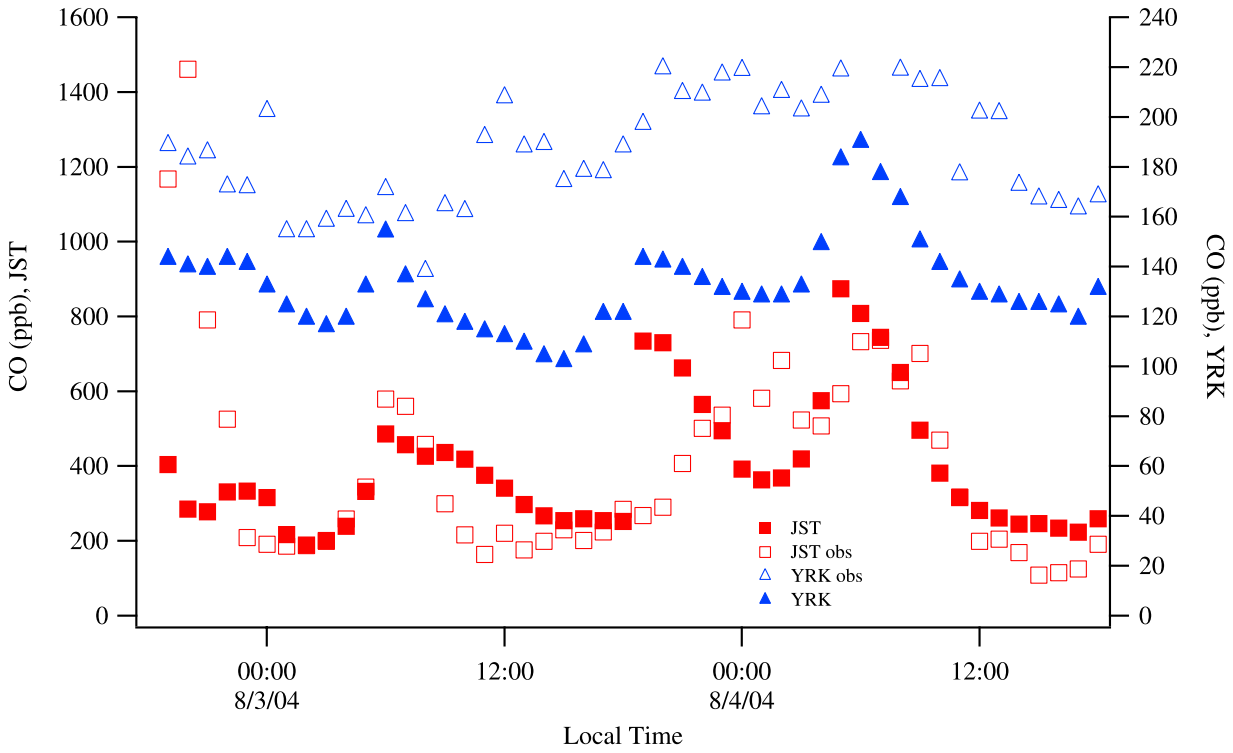

Figure 3d. Base case simulations and observations (obs) of CO mixing ratios in two locations in the southeastern United States associated with the SEARCH network (YRK, Yorkville, Georgia; JST, Jefferson Street, Atlanta, Georgia).

terms of both magnitude and timing of peaks. There are, however, points in time when the model either overpredicts or underpredicts the measured values. Specifically, the large spike in the observed values that occurred at approximately 2100 local time is not captured by the model. These discrepancies may be related to specific plane locations being mapped onto a grid of 36 km in horizontal resolution and varying vertical resolution, the high speed of the plane, imprecision in emissions inventories, and inaccuracies in the simulated mixing and meteorological processes. No effort is made in this study to vary input parameters to better match observations; instead, the best available input defined by SMOKE1.0 and MM5 is used to highlight cases such as this where model performance is not optimal.

[22] The ship track of the *Ronald H. Brown* was concentrated along the coast of southern Maine; again latitude and longitude were used to determine appropriate horizontal grid cells for comparison. A comparison between observations and modeled output for these mobile platforms is given in Figure 3c. An average underprediction on the order of 80 ppb is found for the *Ronald H. Brown*, but the relatively unvarying temporal behavior is adequately mimicked. Explanations for the discrepancy between measured and simulated mixing ratios are similar to those discussed above with respect to Figure 3b. It has been shown previously that the vertical structure of the atmosphere over the Gulf of Maine where the *Ronald H. Brown* sampled is very complex [*Angevine et al.*, 2006], making prediction of its physical characteristics difficult.

[23] For comparison to observations in an additional part of the eastern United States domain, data from two SEARCH sites are used. These sites are Yorkville (YRK), Georgia, a rural site west of Atlanta, Georgia, and Jefferson Street (JST) in urban Atlanta, Georgia. These comparisons are made in Figure 3d. Acceptable agreement in terms of peaks and timing of peaks is indicated for the urban site. At the rural site, significantly less variability is observed in both the simulated mixing ratios and the observed ones; the model underpredicts the observations on average by approximately 50 ppb. Potential explanations for the discrepancies between simulated and observed mixing ratios have been discussed previously.

[24] In the SoCAB, CO concentrations are predicted, on average, to be larger than those in the eastern United States, as shown in Figure 3e. Highest concentrations occur in areas furthest upwind (CELA) because of strong input of automobile emissions. The mixing ratios are smaller moving from west to east (that is, the mixing ratio in CELA is greater than that in AZUS, which is greater than that in RIVR) because of dilution during transport from areas affected strongly by primary emissions. Maxima generally occur at 0600 and 1800 local time at all locations, likely because of rush hour activities, which interestingly occur at earlier hours than do the corresponding peak periods in BS. As in BS, it is difficult to compare observations and simulations because of rounding of measured data. In general, morning rush hour and midday periods are simulated accurately; evening rush hour periods, however, show consistent overpredictions in the more upwind locations. Clearly, the SoCAB is

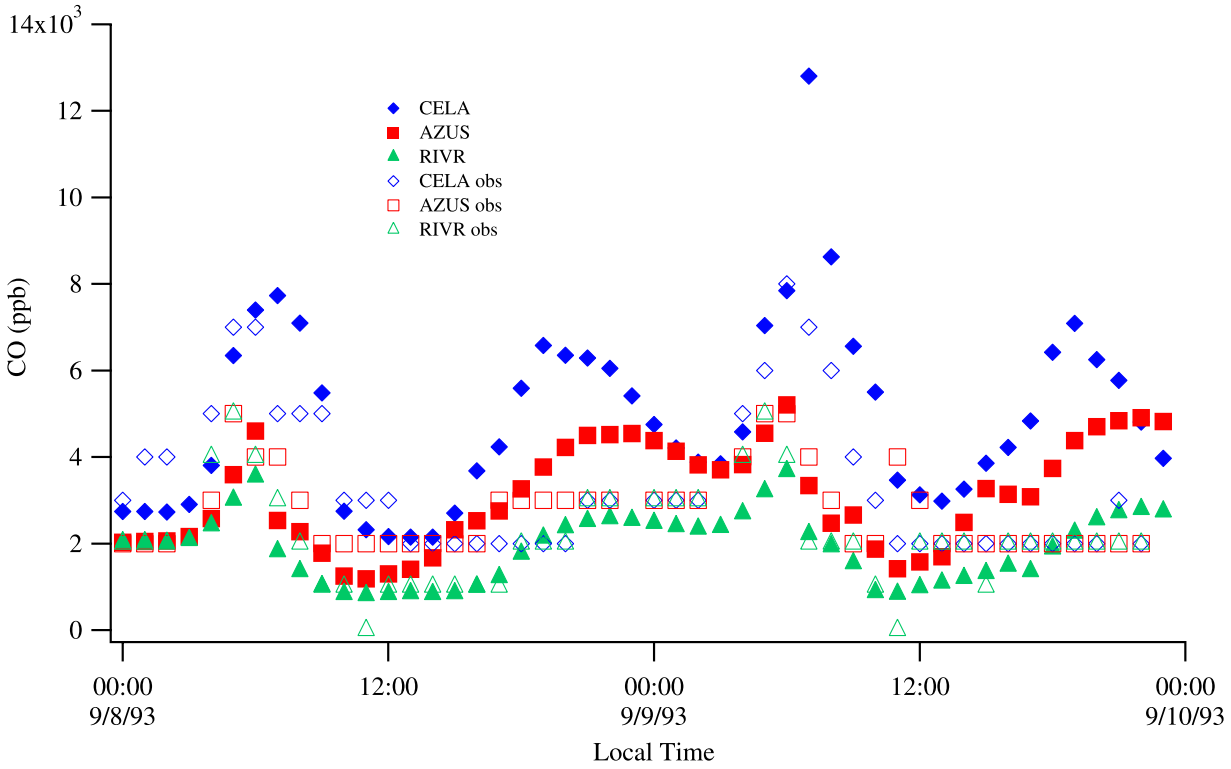

Figure 3e. Base case simulations and observations (obs) of CO mixing ratios in three locations in the SoCAB (CELA, central Los Angeles; AZUS, Azusa; RIVR, Riverside).

significantly more polluted than is the New England region.

[25] Figure 4 shows the base case, model-predicted, 24-hour average CO mixing ratio contour for each of the 2 days of simulation for each of the two domains. In general in the eastern United States, highest values are observed in major metropolitan areas such as Chicago, Illinois; New York City, New York; and Atlanta, Georgia (up to approximately 800 ppb), with the highest maximum occurring in the Chicago area on the first simulation day. On both days, there is a widespread area characterized by mixing ratios between 100 and 200 ppb. The extent of the widespread area is larger and further over the Atlantic Ocean on the second day of the simulation compared to the first day.

[26] In the SoCAB, the 24-hour average CO mixing ratio contour maps indicate very similar profiles for the 2 days, with a small increase in maximum concentration for the second day of simulation. In general, the highest average mixing ratios are observed in CELA with areas of high concentration extending southward toward Anaheim on both days and eastward toward RIVR, particularly on the second day of simulation. This zone characterized by high mixing ratios (approximately 3,000 to 5,000 ppb) is surrounded completely and consistently by areas characterized by sub-1,000-ppb average mixing ratios of CO.

[27] For comparative purposes with Figure 4, emission contour maps for each domain are shown in Figure 5. In the eastern United States, emission hot spots are spatially coincident with major metropolitan areas (Boston, Massachusetts; New York City, New York; Washington, D. C.; Atlanta, Georgia; Chicago, Illinois; Detroit, Michigan; etc.) that experience large contributions to CO emissions from fossil fuel burning by automobiles. The widespread consistency of predicted CO mixing ratios in contrast to the steep gradients associated with the emissions indicates the importance of transport and the relatively long lifetime (an average greater than 2 weeks based on 48-hour, domain-wide averages for this polluted region, indicating relatively high levels of OH) of CO in determining its mixing ratio. A similar comparison for the SoCAB indicates a similar phenomenon. Emissions are concentrated in the western end of the SoCAB around CELA and areas just south and west. Contours of average mixing ratios indicate spreading and dilution to the east, consistent with prevailing wind direction.

3.2. Sensitivity Results

3.2.1. Total VOC Contribution

[28] Tables 2 and 3 list the percent change in 24-hour average CO mixing ratio in each domain for each day of the simulations when the BCs, ICs, and emissions of a given species are set to zero. Information is presented for the domain-wide (DW) average as well as three specific locations within each domain: TF, AI, and BS for New England and CELA, AZUS, and RIVR for the SoCAB. The percent change (Δ) is calculated as:

$$\Delta(\%) = \left(\frac{CO_{sens} - CO_{base}}{CO_{base}}\right)100 \qquad (2)$$

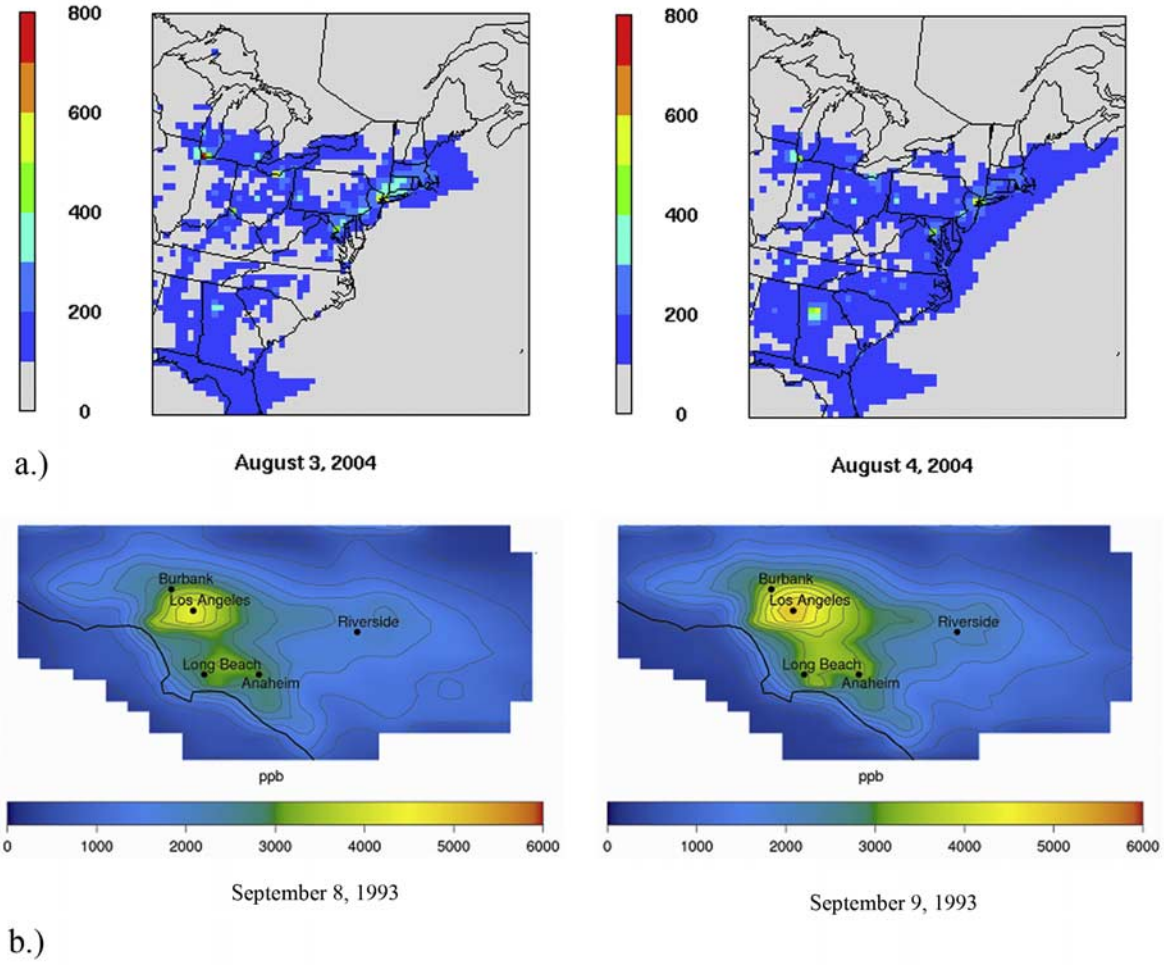

Figure 4. Twenty-four hour average CO mixing ratio (ppb) for each day of the simulations in (a) the eastern United States and (b) the SoCAB.

where CO_i is the domain-wide or grid-box-specific 24-hour averaged mixing ratio in simulation case *i*, *base* represents the base case, and *sens* represents those cases in which emissions, BCs, and ICs are set to zero for a specific species.

[29] In the eastern United States, the contribution of photochemical CO to domain-wide 24-hour average CO mixing ratios is 2.9 and 9.0%, for the first and second simulation day, respectively, on the basis of the case where BCs, ICs, and emissions for CO are set to zero. This case is equivalent to all CO in the domain being generated by the photochemical oxidation of VOCs. The base case, 24-hour average, domain-wide simulated mixing ratios of CO are 89.3 and 90.7 ppb for the first and second day of simulation, respectively. The same values for the case without BCs, ICs, and emissions of CO are 2.6 and 8.2 ppb. Photochemical CO is more important on the second day of the simulation. Given similar emissions on each day, it is clear that meteorological processes influence the photochemical generation of CO (and therefore OH levels as well as the relative ratio of VOCs to NO_x), as does carryover of photochemically generated CO from the previous day. The contribution of photochemical CO from VOC oxidation at given locations ranges from 2.0% (BS on the first day of the simulation) to 6.7% (TF on the second day of the simulation).

[30] Of the individual locations investigated in New England, the larger contributions of photochemical derivation to CO levels occur for TF (2.4 to 6.7%) and AI (2.9 to 5.9%). BS presents a smaller range for the contribution of photochemical generation of CO (2.0 to 4.6%). This is explained by the large influence of biogenic species on OH reactivity at TF [*Griffin et al.*, 2004; White et al., unpublished manuscript, 2007], as well as increased photochemical age during transport from the continent to the marine boundary layer in which AI sits (White et al., unpublished manuscript, 2007).

[31] In the SoCAB, the contribution of the oxidation of VOCs to domain-wide, 24-hour average CO mixing ratios on a percent basis is smaller than that in the eastern United States. The value on each day of the simulation is approximately 1%. The base case, 24-hour average, domain wide mixing ratios are 1,260 and 1,290 ppb for the 2 consecutive days, respectively. Those values for the case without CO are 11.7 and 15.2 ppb, again showing increased importance of photochemical generation of CO on the second day of the simulation, most likely because

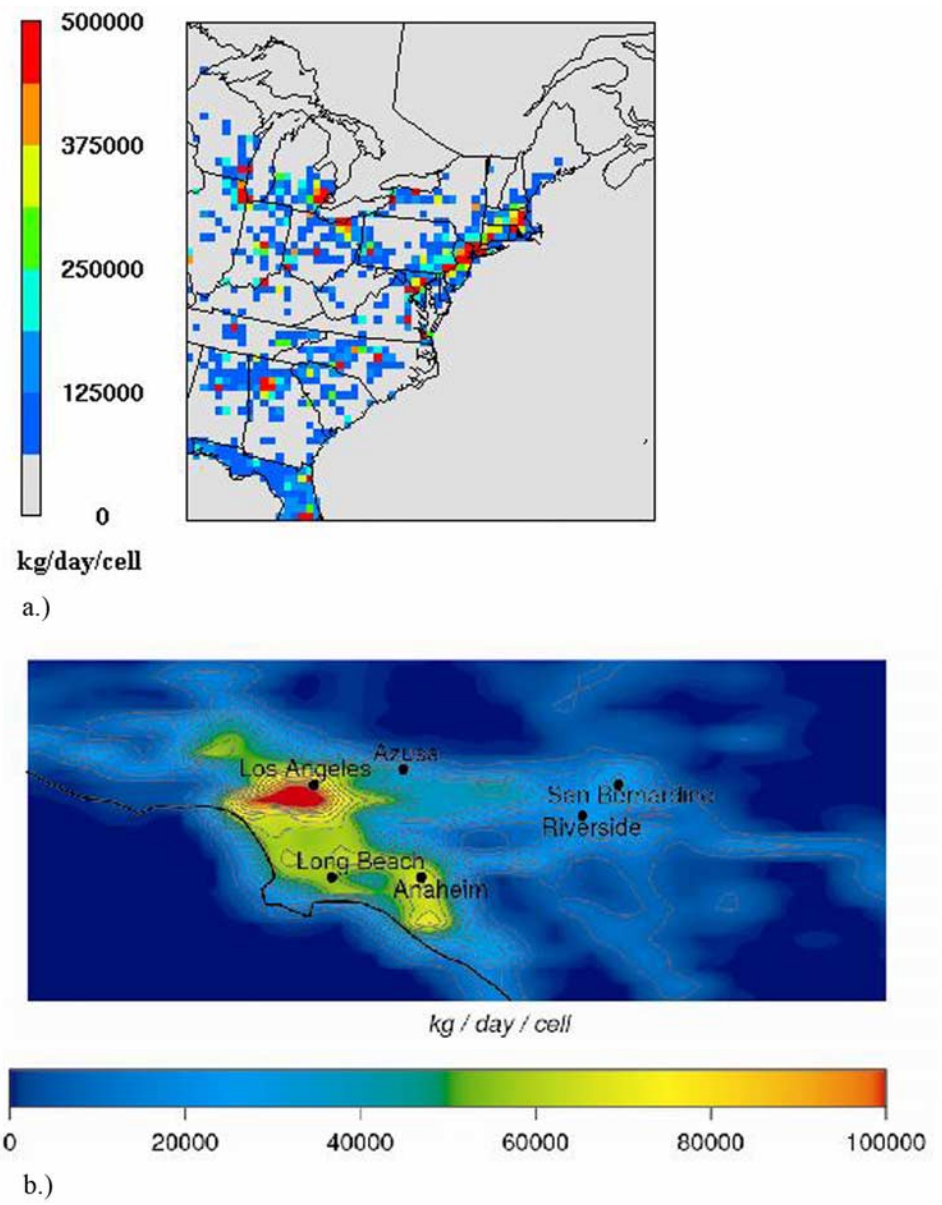

Figure 5. Twenty-four hour average model CO emission rates in (a) the eastern United States and (b) the SoCAB.

of reasons similar to those discussed for the eastern United States. These values are larger than those in the eastern United States despite the smaller domain size (and hence less time for photochemical aging prior to transport out of the domain) because of the large pollutant emission rates in the SoCAB. The effect increases with distance downwind of downtown, indicating increasing effect with photochemical age: CELA (0.3%), AZUS (0.7%), and RIVR (1.0%).

[32] Classification of the total contribution of all VOCs to photochemical CO generation is achieved by setting BCs, ICs, and emissions of CO to zero, as discussed above with respect to Tables 2 and 3. In doing so, however, it must be confirmed that essentially removing most of the CO from the atmosphere within these domains does not affect significantly the overall level of photochemical activity. Figures 6a and 6c indicate the temporal profiles of O_3 in the base cases (compared to observations) and in the simulation without CO for both days of simulation at the three locations of interest in both domains. In both domains, simulation of observations is adequate, as discussed previously [*Griffin et al.*, 2002b; *Chen et al.*, 2006], and little influence of CO on O_3 formation is indicated. Because photolysis of O_3 is expected to be the primary formation pathway for OH in the atmosphere, OH levels are also unlikely to change significantly because reaction (R1) is relatively slow. Therefore photochemical activity (using O_3 and OH levels as proxies) is not likely

Table 2. Percent Change in 24-Hour Average CO Mixing Ratios as Calculated Using Equation (2) When the Boundary Conditions, Initial Conditions, and Emissions of the Species Listed in the First Column Are Set to Zero for the Eastern United States for 3 August (Day 1) and 4 August (Day 2) 2004[a]

Site	DW	DW	TF	TF	AI	AI	BS	BS
Day	1	2	1	2	1	2	1	2
CO	−97.1%	−91.0%	−97.6%	−93.3%	−97.1%	−94.1%	−98.0%	−95.4%
CH_4	−0.8%	−0.8%	−0.5%	0.0%	−0.4%	−0.6%	−0.3%	−0.5%
HCHO	−0.4%	−0.6%	0.0%	0.0%	−0.4%	−0.6%	−0.3%	−0.5%
ETHE	0.0%	0.0%	0.0%	0.0%	−0.4%	−0.6%	0.0%	0.0%
ALKL	0.0%	−0.1%	0.0%	0.0%	−0.4%	−0.6%	0.0%	−0.5%
OLEL	−0.1%	−0.2%	0.0%	0.0%	−0.4%	−0.6%	0.0%	−0.5%
ISOP	−1.0%	−4.1%	−1.0%	−2.2%	−1.2%	−2.3%	−0.7%	−1.9%
ALD2	0.0%	0.0%	0.0%	0.0%	0.0%	−0.6%	0.0%	0.0%
AROL	0.0%	0.0%	0.0%	0.0%	−0.4%	−0.6%	0.0%	0.0%
AROH	0.0%	0.0%	0.0%	0.0%	−0.4%	−0.6%	0.0%	−0.5%

[a]Only species for which the change in at least one location is greater than or equal to ±0.3% are shown. DW refers to domain-wide.

to be altered significantly within these domains for the runs in which BCs, ICs, and emissions of CO are set to zero. This is confirmed by the temporal profiles of OH shown in Figures 6b and 6d that indicate small changes only in the middle of the day in the more downwind locations in the SoCAB (RIVR on day one and AZUS on day two).

[33] To investigate the total VOC contribution to photochemical CO generation on a more regional scale, Figure 7 indicates 24-hour average CO contours for each domain for each day in the case without BCs, ICs, and emissions of CO. Correspondingly, Figure 8 presents 48-hour temporal profiles of CO for the case without BCs, ICs, and emissions of CO in each of the three locations of interest in each domain.

[34] In the eastern United States, Figure 7 shows that the highest photochemical generation of CO occurs in the southwestern corner of the domain in Tennessee, Alabama, and Georgia. These regions are associated with high biogenic emissions. Smaller peaks are observed in the New England region and along the Appalachian Mountains. Specifically focusing on the three chosen locations of interest, Figure 8 indicates that the peak of the mixing ratio of CO that can be attributed to photochemical generation occurs at approximately 1800 local time. Even though the domain-wide influence is larger on the second day, the first day of the simulation experiences higher photochemical CO formation at AI and BS (peaks of 20 and 15 ppb, respectively, compared to 13 and 11 ppb). The influence at TF is less dependent on simulation date. Because domain-wide influences are larger on the second day and emissions inventories are similar, the fact that local influences are smaller in New England indicates the role of local meteorological conditions (transport rates and mixing height).

[35] In the SoCAB, biogenic emissions are relatively minor and anthropogenic emissions, while concentrated to the greatest extent in the western portion of the basin, are widespread. With the prevailing westerly wind, therefore, it is not surprising that the contours of photochemically generated CO indicated in Figure 7 show the highest concentrations in the east, near the edge of the model domain. Average mixing ratios of photochemically generated CO approach 30 to 40 ppb at these maxima. Photochemical generation of CO at the three locations of interest within the SoCAB follow different patterns than those simulated for New England in that peaks tend to occur earlier in the afternoon when photochemistry is strongest, except at the site furthest downwind. In CELA, peaks of photochemically generated CO (approximately 35 ppb) are observed at approximately noon local time, followed by rapid decay as material is transported eastward. AZUS also shows this noon-time peak (35–38 ppb), but with a much less rapid decline, probably associated with transport from upwind locations to counteract transport downwind. Finally, RIVR shows its larger peak in photochemical CO generation (approximately 43 ppb) significantly later in the day

Table 3. Percent Change in 24-Hour Average CO Mixing Ratios as Calculated Using Equation (2) When the Boundary Conditions, Initial Conditions, and Emissions of the Species Listed in the First Column Are Set to Zero for the SoCAB for 8 September (Day 1) and 9 September (Day 2) 1993[a]

Site	DW	DW	CELA	CELA	AZUS	AZUS	RIVR	RIVR
Day	1	2	1	2	1	2	1	2
CO	−99.1%	−98.8%	−99.7%	−99.7%	−99.3%	−99.3%	−99.0%	−99.0%
CH_4	0.0%	−0.1%	0.0%	0.0%	+0.1%	+0.3%	0.0%	−0.1%
ETOH	0.0%	0.0%	−0.3%	+0.1%	−0.1%	+0.3%	0.0%	0.0%
OLEL	−0.2%	−0.3%	0.0%	−0.3%	−0.2%	−0.1%	−0.3%	−0.4%
ISOP	0.0%	0.0%	−0.1%	+0.1%	+0.1%	+0.3%	0.0%	−0.1%
ALD2	0.0%	0.0%	−0.3%	0.0%	0.0%	+0.2%	0.0%	−0.1%
AROL	−0.1%	−0.1%	−0.1%	−0.3%	−0.1%	−0.1%	−0.1%	−0.2%
PAH	0.0%	0.0%	−0.1%	−0.3%	+0.1%	+0.2%	0.0%	−0.1%

[a]Only species for which the change in at least one location is greater than or equal to ±0.3% are shown. DW refers to domain-wide.

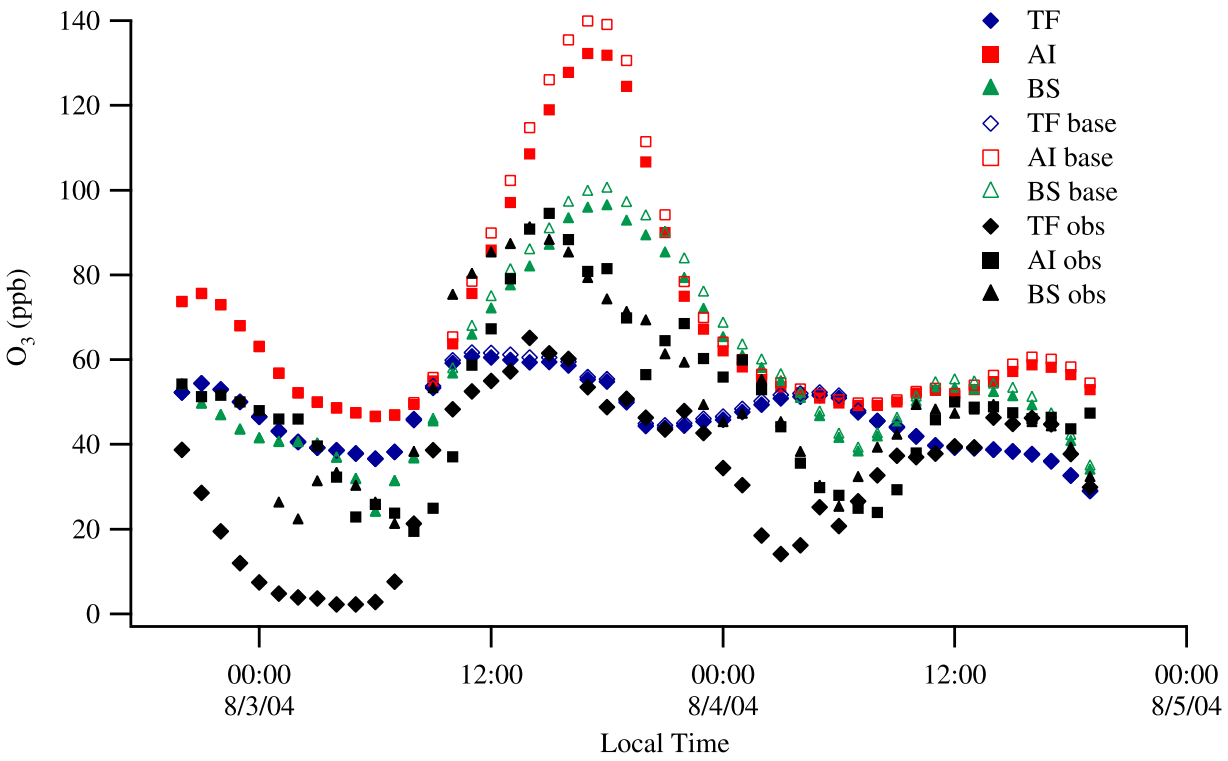

Figure 6a. Base case simulations (base), observations (obs), and simulations in which CO initial conditions, boundary conditions, and emissions are set to zero for O_3 in three locations in New England (TF, Thompson Farm; AI, Appledore Island; BS, Boston, Massachusetts).

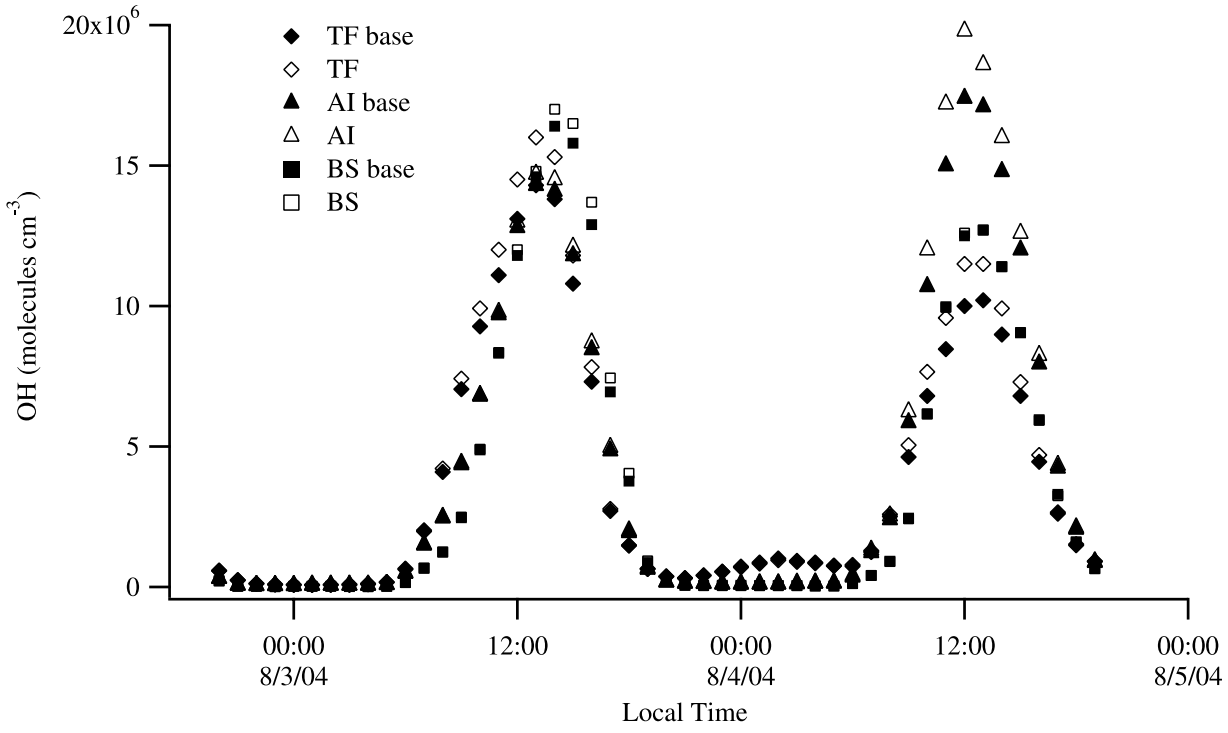

Figure 6b. Simulated OH concentrations in three locations in New England (TF, Thompson Farm; AI, Appledore Island; BS, Boston, Massachusetts) in the base case (base) and the case in which CO initial conditions, boundary conditions, and emissions are set to zero.

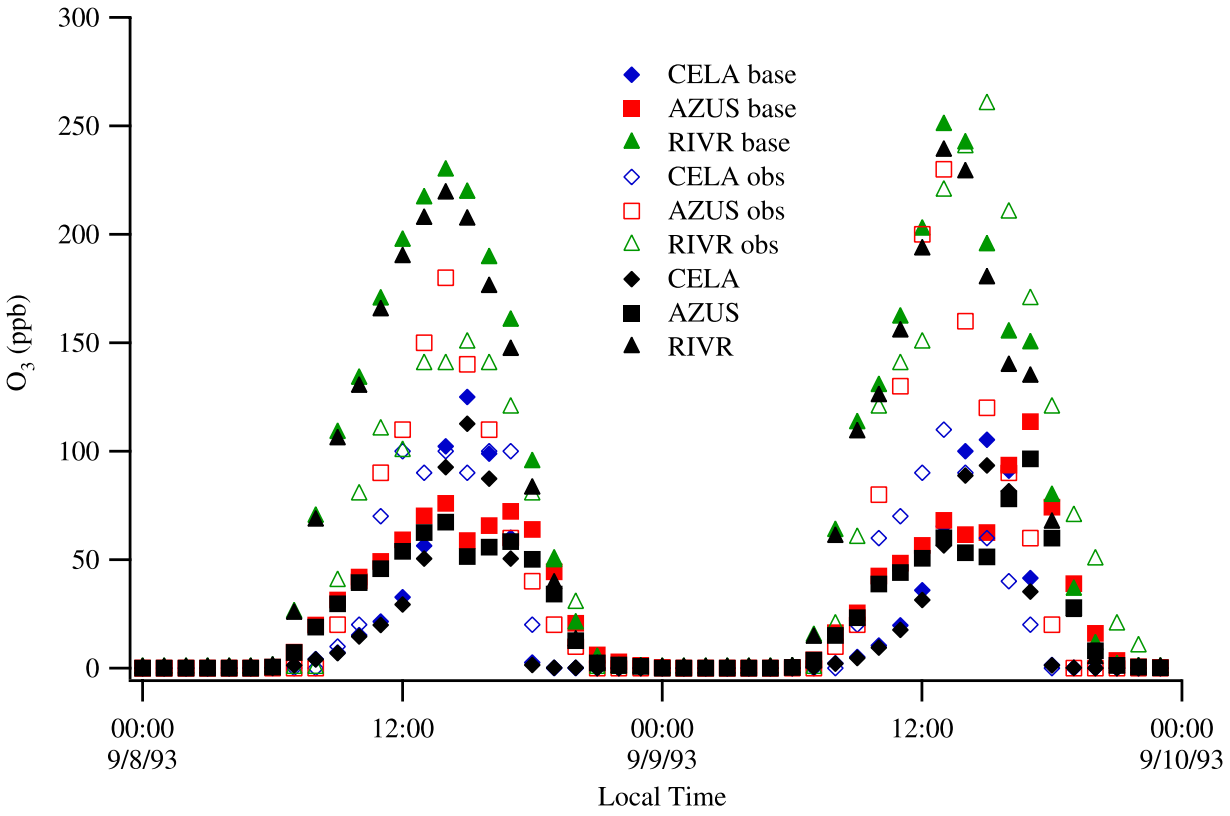

Figure 6c. Base case simulations (base), observations (obs), and simulations in which CO initial conditions, boundary conditions, and emissions are set to zero for O_3 in three locations in the SoCAB (CELA, central Los Angeles; AZUS, Azusa; RIVR, Riverside).

because both VOCs as well as CO generated upwind need to be transported to this location.

3.2.2. Individual VOC Contributions

[36] In addition to understanding how VOCs in concert lead to photochemical generation of CO, the contribution of individual species is also of interest. Sensitivity runs focused on individual species are also described in Tables 2 and 3. Data are included only for those cases in which at least a ±0.3% change is found. For the eastern United States, the only species on a domain-wide basis that photochemically contributes at least 1% to CO levels is ISOP. This occurs on both days of the simulation, with the contribution on the second day being slightly greater than 4%. ISOP is the largest contributor to VOC-derived CO in each of the individual locations in New England as well. Figure 9 shows CO temporal profiles for TF, AI, and BS for the base case and the ISOP-free case. Only small shifts downward are observed in the case when the ICs, BCs, and emissions of ISOP are set to zero.

[37] AI is also characterized by the largest number of species that result in nonzero percent changes when their BCs, ICs, and emissions are set to zero, regardless of day, as shown in Table 2. This is consistent with transport from the continent to the marine boundary layer in which AI sits, allowing for increased photochemical aging during transport. The influences of all species other than ISOP are coincidentally 0.4% or 0.6% at AI for the first and second day of simulation, respectively.

[38] In the SoCAB, on both days of the simulation, the species that contributes the largest amount to photochemical generation of CO on a domain-wide basis is OLEL. However, this contribution is relatively small, 0.2% on the first day and 0.3% on the second. OLEL is also the largest contributor to CO generation at each location on each day (up to 0.4%), except in CELA. On the first day in CELA, ETOH and ALD2 both contribute 0.3%. On the second day in CELA, OLEL and aromatic species each contribute 0.3%. However, the contribution of OLEL is not large enough to be discernable from the base case on a plot of CO mixing ratios that also contains the OLEL sensitivity output, unlike ISOP in the eastern United States.

[39] Unlike the eastern United States, within the SoCAB, removal of certain species in terms of BCs, ICs, and emissions may actually lead to small increases in CO at a given location. This does not occur on a domain-wide average or at RIVR, the site furthest downwind and characterized most strongly by secondary chemistry. In CELA, this occurs with ETOH and ISOP on the second day of the simulation. This phenomenon is much more prevalent at AZUS, the site with mixed influences of primary emissions and secondary chemistry. On the first day, ISOP, CH_4, and PAH omissions lead to slight increases in CO. On the second day, these three species as well as ETOH and ALD2 do so. This phenomenon can be explained by small decreases in O_3 caused by reductions in these VOCs. A simultaneous decrease in OH will occur, leading to an increase in CO due to a decrease in the rate of reaction

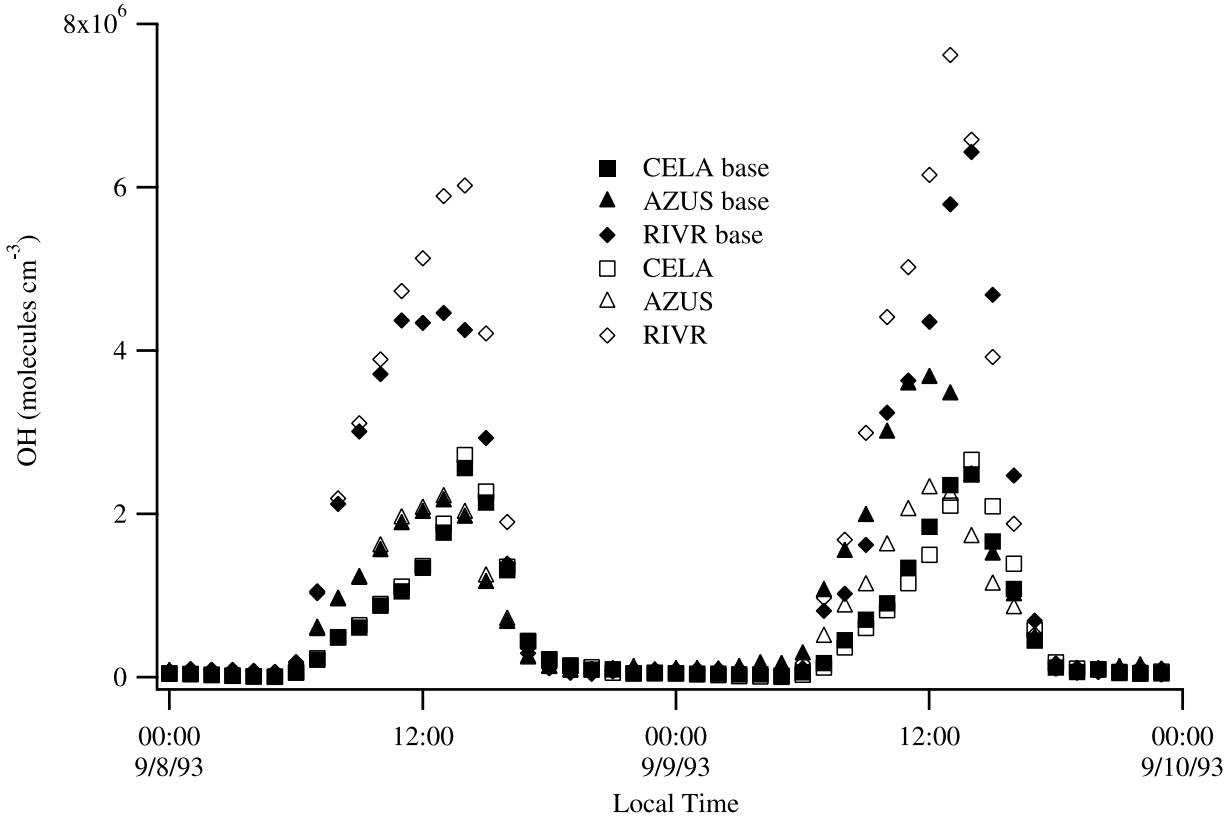

Figure 6d. Simulated OH concentrations in three locations in the SoCAB (CELA, central Los Angeles; AZUS, Azusa; RIVR, Riverside) in the base case (base) and the case in which CO initial conditions, boundary conditions, and emissions are set to zero.

(R1). In these cases, the feedback on the OH-CO reaction is greater than the decrease in the secondary formation of CO caused by the reduction of those VOCs in those sensitivity simulations. In any case, the changes are never greater than a 0.3% increase over the base case.

4. Discussion

4.1. Carbon Monoxide

[40] Approximately 40% of the global annual production rate of CO is derived from the oxidation of CH_4 and other non-CH_4 VOCs. This phenomenon is most prevalent in areas influenced strongly by biogenic emissions and occurs to the greatest extent when conditions are conducive to photochemistry. In contrast to this global average, the fractions presented here for the eastern United States and for the SoCAB (average of approximately 5% and 1%, respectively) are significantly smaller for the high-pollution summer episodes modeled in this study. These differences result for a number of reasons, including the smaller domains used in regional models, meaning that carbon can be transported out of the model domain more rapidly than it is converted to CO, the large local impact of primary CO emissions, and the strong influence of heavily forested regions in South America and Africa on the global average. It should also be noted that the global average cited refers to an annual average where this study focuses on specific episodic events.

[41] On a relative basis, the influence of photochemistry on CO generation would appear to be more important in the eastern United States (average of 5%) than in the SoCAB (average of 1%). This is because of the relatively larger effect of ISOP in the eastern United States and because of the large emission rate of CO in the SoCAB due to fossil fuel burning by automobiles. However, on an absolute scale, the mixing ratio of CO obtained through photochemical generation is larger in the SoCAB. For the three locations of interest in the SoCAB, the 48-hour average generated mixing ratio is 18.2 ppb. The corresponding value for the three locations in New England is 7.3 ppb. Therefore it is important to consider photochemical CO generation regionally on both the absolute and relative scales.

[42] The results of this work are relevant for any calculations that use measured CO as a means to calculate other parameters. For example, one method of calculating OPE is to use the slope of a regression between O_3 and CO because O_3 is purely secondary and CO is mostly primary [*Fishman and Seiler*, 1983; *Griffin et al.*, 2004]. Using this method, the OPE calculated for TF during the New England Air Quality Study (NEAQS) during summer 2002 was 9.7 [*Griffin et al.*, 2004]. The OPE is a measure of how many molecules of O_3 are formed by a molecule of NO_x before the NO_x is removed from the chemical system. However, without correcting for secondary generation of CO, which on average accounts for 5% during summer in New England

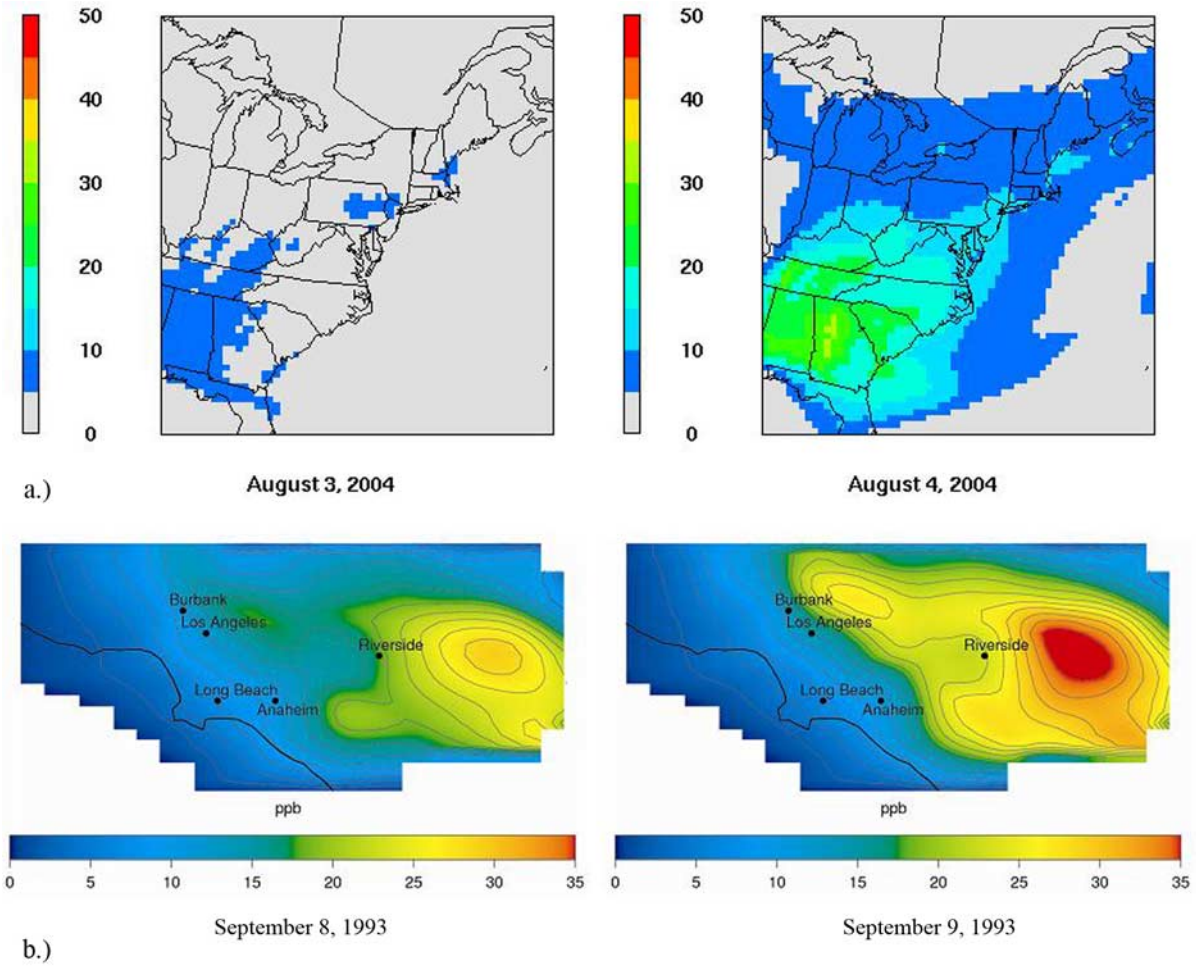

Figure 7. Twenty-four hour average CO mixing ratio (ppb) for each day of the simulations in (a) the eastern United States and (b) the SoCAB for the case in which CO initial conditions, boundary conditions, and emissions are set to zero.

on the basis of the modeling results presented here, this slope will be underestimated by 5%, leading to a 5% underprediction in OPE. A corrected OPE for this region is then 10.2 for the NEAQS time period. This is important if the OPE calculated in this way is used to determine the timing of the seasonal shift from NO_x-limited to VOC-limited chemistry in New England [*Jacob et al.*, 1995].

4.2. Formaldehyde

[43] Similar analyses can also be performed for the major secondary precursor of CO (HCHO) and for CO_2, the oxidation product of the reaction between CO and OH, as described in reaction (R1). Considering HCHO first on a domain-wide basis in the eastern United States, the only species that lead to a greater than 1% decrease in HCHO level when their emissions, BCs, and ICs are set to zero (besides HCHO itself) are ISOP, the monoterpene species, and OLEL. By far the biggest influence on HCHO levels comes from ISOP. When the BCs, ICs, and emissions of ISOP are set to zero, the domain-wide, 24-hour average HCHO mixing ratios decrease by 40.2% and 70.0%, for the first and second day of the simulation for the eastern United States. Anthropogenic species have a much larger effect on HCHO in the SoCAB. Zeroing of ETHE (11–12%) and OLEL (23–25%) leads to significantly larger relative decreases in HCHO in the SoCAB over the 2 days of simulation. Clearly the level of these decreases in HCHO is not carried forward to CO, most likely because it is transported out of the model domains before it is converted to CO.

4.3. Carbon Dioxide

[44] Analysis for CO_2 is significantly more difficult because emission of CO_2 is not included in the modeling analyses and because terrestrial uptake and release of CO_2 are not considered. This indicates that any CO_2 predicted by the model is purely that generated because of photochemistry, either via reaction (R1) or via direct production, primarily via alkene-O_3 reaction or the decomposition of acyl alkoxy radicals (RCO_2). Therefore it is not possible to calculate a relative contribution of photochemistry to total CO_2 on the regional scale in this study. However, it is possible to determine the VOC species that contribute the greatest amount to photochemical generation of CO_2. On a domain-wide average in the eastern United States, the contribution of individual VOCs is negligible; only when the emissions, BCs, and ICs of CO are set to zero does a measurable change result. On an

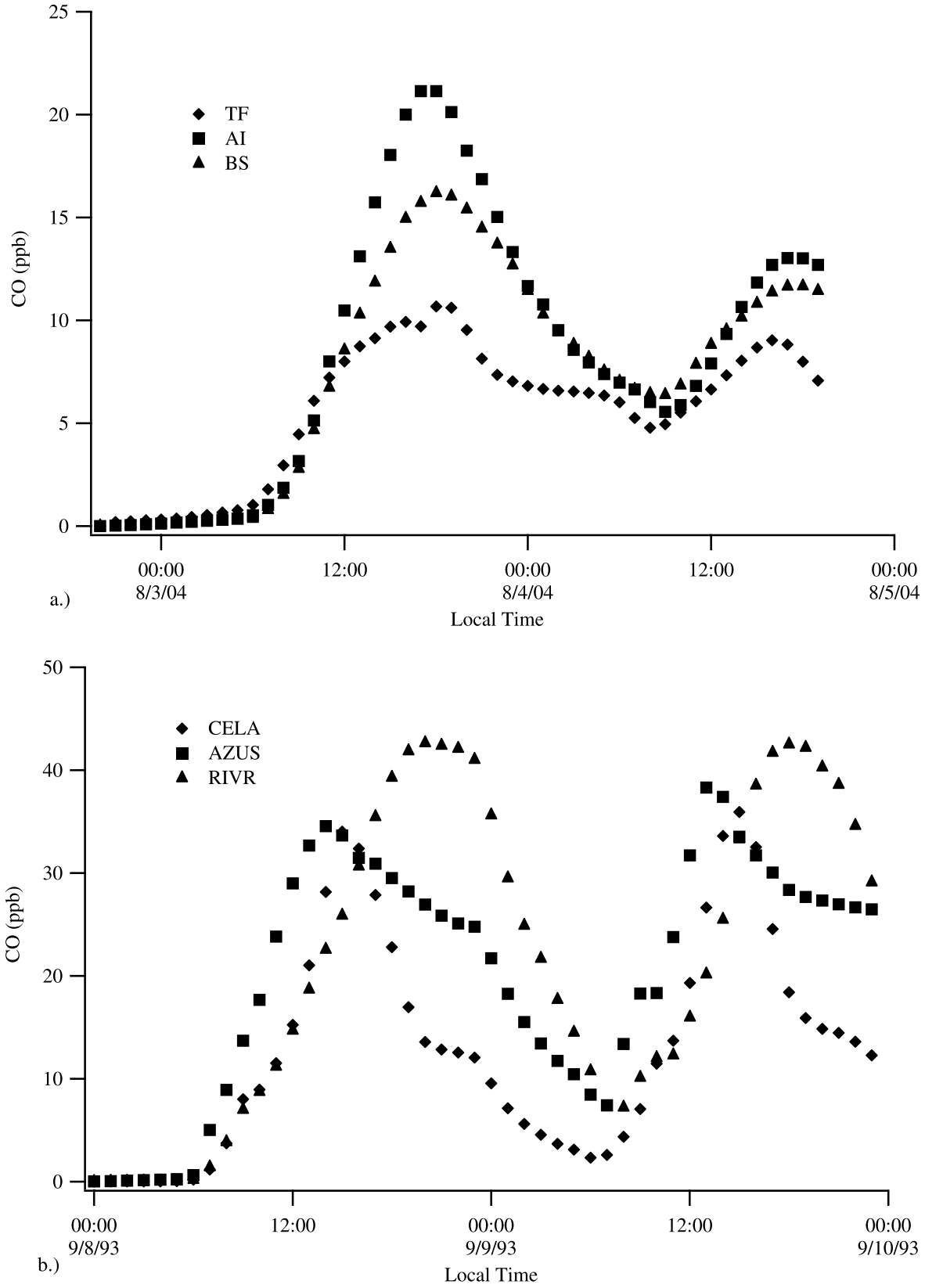

Figure 8. Simulation of CO in three locations in (a) New England (TF, Thompson Farm; AI, Appledore Island; BS, Boston, Massachusetts) and (b) the SoCAB (CELA, central Los Angeles; AZUS, Azusa; RIVR, Riverside) when initial conditions, boundary conditions, and emissions of CO are set to zero.

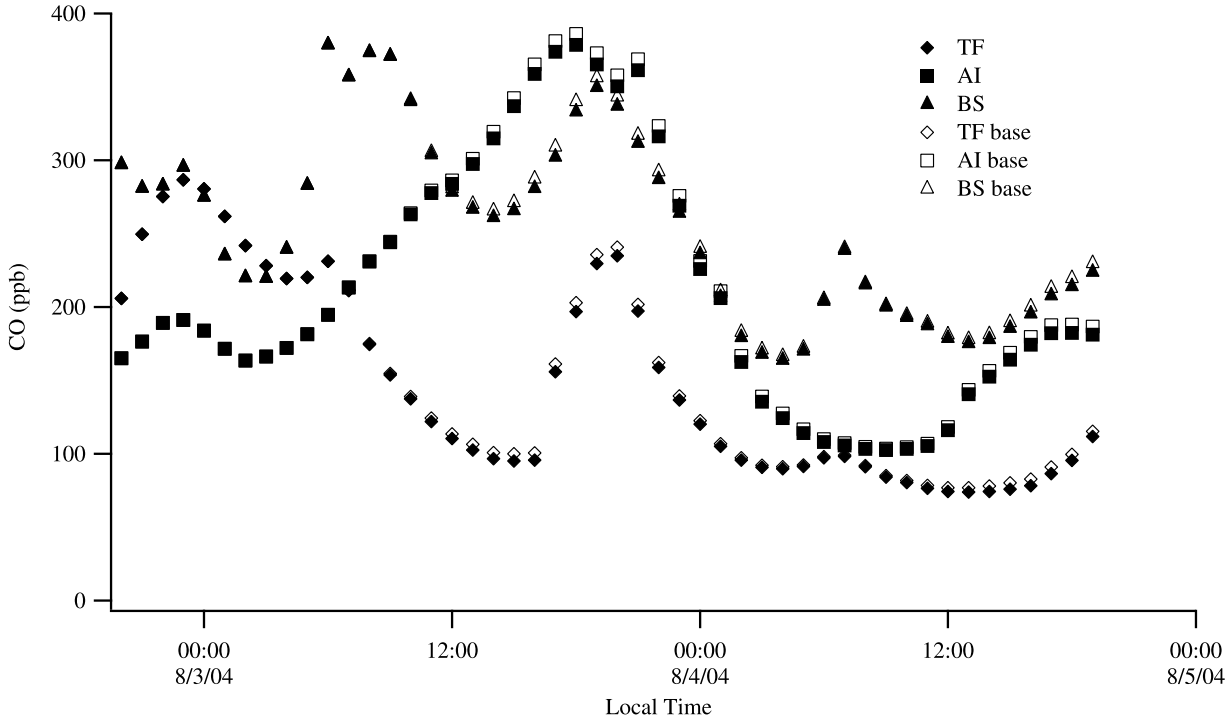

Figure 9. Simulation of CO in three locations in New England (TF, Thompson Farm; AI, Appledore Island; BS, Boston, Massachusetts) when initial conditions, boundary conditions, and emissions of isoprene are set to zero. Base case simulation output is shown with open symbols.

individual location basis, not surprisingly, ISOP has the largest effect on relative photochemical CO_2 generation (up to a 7.2% decrease) at AI. In contrast, domain-wide averages of photochemical CO_2 generation are affected significantly by individual species in the SoCAB. Species that exhibit a decrease in CO_2 of greater than 10% when their emissions, BCs, and ICs are set to zero include OLEL (24–26%), ALD2 (11.3%), AROH (10.3–11.1%), and AROL (11.2–11.8%).

5. Conclusions

[45] This study indicates the importance of VOC oxidation to secondary CO generation through the use of modeling studies in two different locations for two different time periods. While the percent contribution of VOC oxidation to the CO levels is small, the absolute mixing ratio is as high as 40 ppb, depending on time and date. In addition, the relative amounts may be significant enough to imply that studies that use measured CO as a marker of combustion emission should account for its photochemical generation. If secondary contributions are ignored, any parameters derived from measured CO under the assumption that CO is purely primary will also be estimated incorrectly. It is recommended that such studies correct for CO photochemical generation in the future. It is also recommended that calculations such as those presented here are repeated in the future as anthropogenic emissions change, biogenic emissions are altered by global warming and changes in land cover, and our understanding of VOC oxidation pathways increase.

[46] **Acknowledgments.** Financial support for this work was provided by the Office of Oceanic and Atmospheric Research of NOAA under AIRMAP grants NA03OAR4600122 and NA04OAR4600154. Any opinions, findings, and conclusions or recommendations expressed in this material are those of the authors and do not necessarily reflect the views of the funding agency. The authors would also like to thank Huiting Mao for provision of model input files for the eastern United States, Bob Talbot for useful discussion, and the AIRMAP project team for continued operation and maintenance of the UNH Atmospheric Observatories. The provision of CO data by Mike Kleeman (SoCAB), Wendy McDougall (Boston), Brian Lerner (Research Vessel *Ronald H. Brown*), and John Holloway (NOAA P-3 aircraft) is greatly appreciated, as is the assistance of Wayne Chang in generation of figures.

References

Anderson, B. E., G. L. Gregory, J. D. W. Barrick, J. E. Collins, G. W. Sachse, D. Bagwell, M. C. Shipham, J. D. Bradshaw, and S. T. Sandholm (1993), The impact of United States continental outflow on ozone and aerosol distributions over the Western Atlantic, *J. Geophys. Res.*, *98*, 23,477–23,489.

Angevine, W. M., M. Tjernstrom, and M. Zagar (2006), Modeling of the coastal boundary layer and pollutant transport in New England, *J. Appl. Meteorol. Climatol.*, *45*, 137–154.

Binkowski, F. S., and S. J. Roselle (2003), Models-3 Community Multiscale Air Quality (CMAQ) model aerosol component: 1. Model description, *J. Geophys. Res.*, *108*(D6), 4183, doi:10.1029/2001JD001409.

Byun, D. W., and J. K. S. Ching (1999), Science algorithms of the EPA Models-3 Community Multiscale Air Quality (CMAQ) modeling system, *Rep. EPA/600/R-99/030*, Off. of Res. and Dev., U.S. Environ. Prot. Agency, Washington, D. C.

Chen, J., and R. J. Griffin (2005), Modeling secondary organic aerosol formation from α-pinene, β-pinene, and d-limonene, *Atmos. Environ.*, *39*, 7731–7744.

Chen, J., H. Mao, R. W. Talbot, and R. J. Griffin (2006), Application of the CACM and MPMPO modules using the CMAQ model for the eastern United States, *J. Geophys. Res.*, *111*, D23S25, doi:10.1029/2006JD007603.

Chin, M., D. J. Jacob, J. W. Munger, D. D. Parrish, and B. G. Doddridge (1994), Relationship of ozone and carbon monoxide over North America, *J. Geophys. Res.*, *99*, 14,565–14,573.

de Reus, M., H. Fischer, F. Arnold, J. de Gouw, R. Holzinger, C. Warneke, and J. Williams (2003), On the relationship between acetone and carbon monoxide in different air masses, *Atmos. Chem. Phys.*, *3*, 1709–1723.

Fehsenfeld, F. C., et al. (2006), International Consortium for Atmospheric Research on Transport and Transformation (ICARTT): North America to Europe—Overview of the 2004 summer field study, *J. Geophys. Res.*, *111*, D23S01, doi:10.1029/2006JD007829.

Fishman, J., and W. Seiler (1983), Correlative nature of ozone and carbon monoxide in the troposphere: Implications for the tropospheric ozone budget, *J. Geophys. Res.*, *88*, 3662–3670.

Folberth, G., D. A. Hauglustaine, P. Ciais, and J. Lathière (2005), On the role of atmospheric chemistry in the global CO_2 budget, *Geophys. Res. Lett.*, *32*, L08801, doi:10.1029/2004GL021812.

Fraser, M. P., D. Grosjean, E. Grosjean, R. A. Rasmussen, and G. R. Cass (1996), Air quality model evaluation data for organics: 1. Bulk chemical composition and gas/particle distribution factors, *Environ. Sci. Technol.*, *30*, 1731–1743.

Gery, M. W., G. Z. Whitten, J. P. Killus, and M. C. Dodge (1989), A photochemical kinetics mechanism for urban and regional scale computer modeling, *J. Geophys. Res.*, *94*, 12,925–12,956.

Granier, C., G. Petron, J. F. Müller, and G. Brasseur (2000), The impact of natural and anthropogenic hydrocarbons on the tropospheric budget of carbon monoxide, *Atmos. Environ.*, *34*, 5255–5270.

Griffin, R. J., D. Dabdub, and J. H. Seinfeld (2002a), Secondary organic aerosol: 1. Atmospheric chemical mechanism for production of molecular constituents, *J. Geophys. Res.*, *107*(D17), 4332, doi:10.1029/2001JD000541.

Griffin, R. J., D. Dabdub, M. J. Kleeman, M. P. Fraser, G. R. Cass, and J. H. Seinfeld (2002b), Secondary organic aerosol: 3. Urban/regional scale model of size- and composition-resolved aerosols, *J. Geophys. Res.*, *107*(D17), 4334, doi:10.1029/2001JD000544.

Griffin, R. J., C. A. Johnson, R. W. Talbot, H. Mao, R. S. Russo, Y. Zhou, and B. C. Sive (2004), Quantification of ozone formation metrics at Thompson Farm during the New England Air Quality Study (NEAQS) 2002, *J. Geophys. Res.*, *109*, D24302, doi:10.1029/2004JD005344.

Griffin, R. J., D. Dabdub, and J. H. Seinfeld (2005), Development and initial evaluation of a dynamic species-resolved model for gas-phase chemistry and size-resolved gas/particle partitioning associated with secondary organic aerosol formation, *J. Geophys. Res.*, D05304, doi:10.1029/2004JD005219.

Gros, V., K. Tsigaridis, B. Bonsang, M. Kanakidou, and C. Pio (2002), Factors controlling the diurnal variation of CO above a forested area in southeast Europe, *Atmos. Environ.*, *36*, 3127–3135.

Haan, D., Y. Zuo, V. Gros, and C. A. M. Brenninkmeijer (2001), Photochemical production of carbon monoxide in snow, *J. Atmos. Chem.*, *40*, 217–230.

Hansen, D. A., E. S. Edgerton, B. E. Hartsell, J. J. Jansen, N. Kandasamy, G. M. Hidy, and C. L. Blanchard (2003), The Southeastern Aerosol Research and Characterization Study: Part 1—Overview, *J. Air Waste Manage. Assoc.*, *53*, 1460–1471.

Harley, R. A., A. G. Russell, G. J. McRae, G. R. Cass, and J. H. Seinfeld (1993), Photochemical modeling of the Southern California Air Quality Study, *Environ. Sci. Technol.*, *27*, 378–388.

Harriss, R. C., G. W. Sachse, G. F. Hill, L. O. Wade, and G. L. Gregory (1990), Carbon monoxide over the Amazon basin during the wet season, *J. Geophys. Res.*, *95*, 16,927–16,932.

Houweling, S., F. Dentener, and J. Lelieveld (1998), The impact of nonmethane hydrocarbon compounds on tropospheric photochemistry, *J. Geophys. Res.*, *103*, 10,673–10,696.

Jacob, D. J., L. W. Horowitz, J. W. Munger, B. G. Heikes, R. R. Dickerson, R. S. Artz, and W. C. Keene (1995), Seasonal transition from NO_x- to hydrocarbon-limited regimes for ozone production over the eastern United States in September, *J. Geophys. Res.*, *100*, 9315–9324.

Jenkin, M. E., S. M. Saunders, V. Wagner, and M. J. Pilling (2003), Protocol for the development of the master chemical mechanism, MCMv3 (part B): Tropospheric degradation of aromatic volatile organic compounds, *Atmos. Chem. Phys.*, *3*, 181–193.

Kanakidou, M., and P. J. Crutzen (1999), The photochemical source of carbon monoxide: Importance, uncertainties, and feedbacks, *Chemosphere Global Change Sci.*, *1*, 91–109.

Khalil, M. A. K., and R. Rasmussen (1990), The global cycle of carbon monoxide: Trends and mass balance, *Chemosphere*, *20*, 227–242.

Mao, H., and R. Talbot (2004), O_3 and CO in New England: Temporal variations and relationships, *J. Geophys. Res.*, *109*, D21304, doi:10.1029/2004JD004913.

Mao, H., R. Talbot, D. Troop, R. Johnson, S. Businger, and A. M. Thompson (2006), Smart balloon observations over the North Atlantic: O_3 data analysis and modeling, *J. Geophys. Res.*, *111*, D23S56, doi:10.1029/2005JD006507.

Meng, Z., D. Dabdub, and J. H. Seinfeld (1998), Size-resolved and chemically resolved model of atmospheric aerosol dynamics, *J. Geophys. Res.*, *103*, 3419–3435.

Parrish, D. D., M. Trainer, J. S. Holloway, J. E. Yee, M. S. Warshawsky, F. C. Fehsenfeld, G. L. Forbes, and J. L. Moody (1998), Relationships between ozone and carbon monoxide at surface sites in the North Atlantic region, *J. Geophys. Res.*, *103*, 13,357–13,376.

Poisson, N., M. Kanakidou, and P. J. Crutzen (2000), Impact of nonmethane hydrocarbons on tropospheric chemistry and the oxidizing power of the global troposphere: 3-dimensional modelling results, *J. Atmos. Chem.*, *36*, 157–230.

Seinfeld, J. H. and S. N. Pandis (2006), *Atmospheric Chemistry and Physics: From Air Pollution to Climate Change*, John Wiley, Hoboken, N. J.

Taylor, J. A., P. R. Zimmerman, and D. J. Erickson III (1996), A 3-D modelling study of the sources and sinks of atmospheric carbon monoxide, *Ecol. Model.*, *88*, 53–71.

Tsigaridis, K., and M. Kanakidou (2002), Importance of volatile organic compounds photochemistry over a forested area in central Greece, *Atmos. Environ.*, *36*, 3137–3146.

Zimmerman, P. R., R. B. Chatfield, J. Fishman, P. J. Crutzen, and P. L. Hanst (1978), Estimates on the production of CO and H_2 from the oxidation of hydrocarbon emissions from vegetation, *Geophys. Res. Lett.*, *5*, 679–682.

K. Carmody, D. Dabdub, and S. Vutukuru, Department of Mechanical and Aerospace Engineering, University of California, Irvine, CA 92697, USA.

J. Chen and R. J. Griffin, Climate Change Research Center, University of New Hampshire, Durham, NH 03824, USA. (rob.griffin@unh.edu)